AIP | The Journal of Chemical Physics

Effect of hydrodynamic correlations on the dynamics of polymers in dilute solution

Chien-Cheng Huang, Gerhard Gompper, and Roland G. Winkler

Citation: J. Chem. Phys. **138**, 144902 (2013); doi: 10.1063/1.4799877
View online: http://dx.doi.org/10.1063/1.4799877
View Table of Contents: http://jcp.aip.org/resource/1/JCPSA6/v138/i14
Published by the American Institute of Physics.

Effect of hydrodynamic correlations on the dynamics of polymers in dilute solution

Chien-Cheng Huang,[a] Gerhard Gompper,[a] and Roland G. Winkler[a]
Theoretical Soft Matter and Biophysics, Institute of Complex Systems and Institute for Advanced Simulation, Forschungszentrum Jülich, D-52425 Jülich, Germany

(Received 5 February 2013; accepted 22 March 2013; published online 11 April 2013)

We analyze the effect of time-dependent hydrodynamic interactions on the dynamics of flexible polymers in dilute solution. In analytical calculations, the fluctuating hydrodynamics approach is adopted to describe the fluid, and a Gaussian model to represented the polymer. Simulations are performed exploiting the multiparticle collision dynamics approach, a mesoscale hydrodynamic simulation technique, to explicitly describe the fluid. Polymer center-of-mass velocity correlation functions are calculated for various polymer lengths. Similarly, segment mean square displacements are discussed and polymer diffusion coefficients are determined. Particular attention is paid to the influence of sound propagation on the various properties. The simulations reveal a strong effect of hydrodynamic interactions. Specifically, the time dependence of the center-of-mass velocity correlation functions is determined by polymer properties over a length-dependent time window, but are asymptotically solely governed by fluid correlations, with a long-time tail decaying as $t^{-3/2}$. The correlation functions are heavily influenced by sound modes for short polymers, an effect which gradually disappears with increasing polymer length. We find excellent agreement between analytical and simulation results. This allows us to provide a theory-based asymptotic value for the polymer diffusion coefficient in the limit of large system sizes, which is based on a single finite-system-size simulation.
 [http://dx.doi.org/10.1063/1.4799877]

I. INTRODUCTION

The study of the dynamics of polymers in dilute solution by analytical theory[1–16] and computer simulations[17–31] has a long history. By now, the fundamental importance of fluid-mediated interactions, i.e., hydrodynamic interactions,[7,10] which strongly affect or even dominate the polymer dynamics, is generally accepted and confirmed by experiments on synthetic[7,32–37] and biological flexible and semiflexible polymers.[12,38–43] Moreover, recent fluorescence correlation spectroscopy (FCS) investigations of the dynamics of DNA[44–47] and actin filaments[48,49] as well as fluorescence microscopy studies of DNA[50–52] and actin filaments[53] corroborate the presence and significance of hydrodynamic interactions.

Typically, long time and large scale aspects of the polymer dynamics are discussed. Comparably little attention has been paid to the polymer dynamics on shorter time scales, where fluid fluctuations are important.[54,55] On this scale, polymer center-of-mass velocity correlation functions exhibit a distinct behavior over a wide, polymer-length dependent, time range before the asymptotic long-time tail is reached. Moreover, sound may play an important role on such time scales, depending on the properties of the solvent.

Recent combined experimental, theoretical, and simulation studies of a trapped colloidal particle in solution reveal the effect of hydrodynamic fluctuations and correlations on the colloid dynamics.[56] As has been shown, the fluid "memory" leads to colored, non-white, thermal fluctuating forces,[56] i.e., hydrodynamic self-interactions lead to a self-awareness of the colloidal particle.[57]

Another aspect discussed for colloid dynamics is backtracking.[58–60] For compressible fluids and sufficiently small objects, the colloid motion may induce sound waves, which in turn lead to a reaction force that strongly influences its dynamics. This behavior resembles viscoelasticity and has been theoretically predicted for non-viscoelastic fluids.[58] Measurements suggest that such hydrodynamic correlations appear in many-body systems on time scales shorter than the time needed for vorticity, i.e., shear waves, to diffuse between the colloids.[61] Such aspects have not been addressed for polymers in solution, but polymers should exhibit similar features. To gain insight into the polymer dynamics, we perform mesoscale hydrodynamic simulations by combining the multiparticle collision dynamics (MPC) approach for the fluid with molecular dynamics simulations (MD) for polymers.[62–64] MPC is a particle-based simulation technique which incorporates thermal fluctuations, provides hydrodynamic correlations, and is easily coupled with other simulation techniques such as molecular dynamics simulations for embedded particles.[63–65] It has successfully been applied to study equilibrium and non-equilibrium dynamical properties of colloids,[56,59,63,64,66–73] polymers,[25,29,31,63,64,74–76] vesicles,[77] and red blood cells.[78]

MPC proceeds in two steps—a streaming and a collision step. Collisions occur at discrete times with a fixed interval, and although space is discretized into a lattice of cubic cells

[a]Electronic addresses: c.c.huang@fz-juelich.de; g.gompper@fz-juelich.de; and r.winkler@fz-juelich.de

to define the stochastic collision environment, both particle coordinates and velocities are continuous variables. Various schemes for the multiparticle collision interaction have been proposed.[62–64,79,80] The original method, which employs rotation of relative velocities, is often denoted as stochastic rotation dynamics (SRD).[62–64,79]

In this article, we elucidate the effect of hydrodynamic correlations on the dynamics of polymers in dilute solution. Simulations results are presented, which are obtained by the MPC approach for the fluid. In addition, the fluctuating hydrodynamics approach based on the linearized Landau-Lifshitz Navier-Stokes equation is adopted to derive corresponding theoretical expressions.[65,81] This approach has been shown to describe the emergent fluctuating hydrodynamic of the MPC fluid very well.[65] As far as the polymer dynamics is concerned, the fluctuating hydrodynamic approach has been used in Refs. 54 and 55 for incompressible fluids. We will use a somewhat different approach, adapted to the considered MPC fluid, and consider compressible fluids. Naturally, we will recover some of the previously derived results.

We discuss the center-of-mass velocity correlation functions for polymers of various lengths, considering both, Gaussian phantom chains as well as self-avoiding polymers with bonds of finite length. In addition, diffusion coefficients are determined and a procedure is suggested to obtained the asymptotic infinite-systems-size diffusion coefficients by exploiting the analytical solution for the fluid velocity correlation function. Moreover, the polymer segmental dynamics is analyzed and the scaling properties are determined. Our study reaches far beyond previous ones,[54,55] since we consider both vorticity and sound effects, and present a detail study of chain length and excluded-volume effects.

The paper is organized as follows. In Sec. II, the fluctuating hydrodynamic approach for the MPC fluid is presented and fluid correlation functions are calculated. In Sec. III, the analytical model for the polymer is presented and solutions for its center-of-mass velcocity correlation functions are discussed. Section IV presents the simulation models for the polymer and the fluid. Simulation results of the polymer dynamics are discussed and compared with the analytical theory in Sec. V. Finally, Sec. VI summarizes our findings. An appendix presents more detailed calculations of fluid correlation fluctuations, the hydrodynamic tensor, and velocity correlation functions of self-avoiding polymers.

II. FLUCTUATING HYDRODYNAMICS

The hydrodynamic properties of the MPC fluid are described by the linearized Navier-Stokes equations on sufficiently large length and long time scales.[62–65,82,83] A recent detailed study of the emergent fluctuating hydrodynamics of the MPC fluid even demonstrates that the linearized Landau-Lifshitz Navier-Stokes equations provide an excellent description on length scales above a few collision cells.[65]

For an compressible isothermal MPC fluid, more precisely a SRD fluid, the corresponding linearized continuity and Landau-Lifshitz Navier-Stokes equations are

$$\frac{\partial}{\partial t}\delta\rho + \rho\nabla\cdot\boldsymbol{v} = 0, \tag{1}$$

$$\rho\frac{\partial}{\partial t}\boldsymbol{v} = -\nabla p + \eta\Delta\boldsymbol{v} + \frac{1}{3}\eta^{\mathrm{k}}\nabla(\nabla\cdot\boldsymbol{v}) + \boldsymbol{f}^{c} + \boldsymbol{f}^{R} \tag{2}$$

in three dimensions.[65,81] Here, $\rho + \delta\rho(\boldsymbol{r},t)$ denotes the mass density with its mean value ρ and its (small) fluctuations $\delta\rho(\boldsymbol{r},t)$ at the position $\boldsymbol{r}$ in space and the time t. $\boldsymbol{v} = \boldsymbol{v}(\boldsymbol{r},t)$ is the fluid velocity field, $\boldsymbol{f}^{c}(\boldsymbol{r},t)$ is a volume force, and $\boldsymbol{f}^{R}(\boldsymbol{r},t) = \nabla\cdot\boldsymbol{\sigma}^{R}(\boldsymbol{r},t)$ is the random force due to the thermal fluctuations of the fluid, with $\boldsymbol{\sigma}^{R}$ the corresponding stress tensor. Note that only the mean density ρ will appear throughout the rest of the paper. $\eta = \eta^{\mathrm{k}} + \eta^{\mathrm{c}}$ is the shear viscosity of the MPC fluid, with the kinetic and collisional contributions η^{k} and η^{c}, respectively.[65,83,84] The bulk viscosity is set to zero, in agreement with simulation results[65,83] and expectations for an ideal monatomic gas.[85]

The stochastic process for $\boldsymbol{\sigma}^{R}(\boldsymbol{r},t)$ is assumed to be Gaussian and Markovian with the moments

$$\begin{aligned}\langle\boldsymbol{\sigma}^{R}(\boldsymbol{r},t)\rangle &= 0,\\ \left\langle\sigma^{R}_{\alpha\beta}(\boldsymbol{r},t)\sigma^{R}_{\alpha'\beta'}(\boldsymbol{r},t)\right\rangle &= 2k_BT\eta_{\alpha\beta\alpha'\beta'}\delta(\boldsymbol{r}-\boldsymbol{r}')\delta(t-t'),\end{aligned} \tag{3}$$

where $\alpha,\alpha',\beta,\beta' \in \{x,y,z\}$, and

$$\begin{aligned}\eta_{\alpha\beta\alpha'\beta'} = {}& \eta\delta_{\alpha\alpha'}\delta_{\beta\beta'} + \frac{1}{2}[\eta+\eta^{\mathrm{k}}]\delta_{\alpha\beta'}\delta_{\alpha'\beta}\\ & - \frac{1}{2}\left[\eta + \frac{1}{3}\eta^{\mathrm{k}}\right]\delta_{\alpha\beta}\delta_{\alpha'\beta'}\,.\end{aligned} \tag{4}$$

Since SRD is not conserving angular momentum in the MPC collision step, the fluid stress tensor is non-symmetric,[65,82,83] which is accounted for in the correlations (3). The Navier-Stokes equations and correlation functions of Refs. 54 and 81 for angular momentum conserving fluids are recovered in Eq. (4) for $\eta^{c} = 0$ and $\eta = \eta^{k}$.

The linear Eqs. (1) and (2) are solved by Fourier transformation. Since we want to compare the analytical with computer simulation results, we adopt a discrete Fourier transformation for a spatially periodic and cubic system, i.e., we use[65]

$$\boldsymbol{v}(\boldsymbol{r},t) = \frac{1}{2\pi}\sum_{\boldsymbol{k}}\int\boldsymbol{v}(\boldsymbol{k},\omega)e^{-i\boldsymbol{k}\cdot\boldsymbol{r}}e^{i\omega t}d\omega, \tag{5}$$

$$\boldsymbol{v}(\boldsymbol{k},\omega) = \frac{1}{V}\int\boldsymbol{v}(\boldsymbol{r},t)e^{i\boldsymbol{k}\cdot\boldsymbol{r}}e^{-i\omega t}d^3r\,dt \tag{6}$$

with $k_\alpha = 2\pi n_\alpha/L$, $n_\alpha \in \mathbb{Z}\backslash\{0\}$, and $V = L^3$. As shown in Ref. 65, the resulting flow field is

$$\boldsymbol{v}(\boldsymbol{k},\omega) = \mathbf{Q}(\boldsymbol{k},\omega)[\boldsymbol{f}^{R}(\boldsymbol{k},\omega) + \boldsymbol{f}^{c}(\boldsymbol{k},\omega)] \tag{7}$$

with $\mathbf{Q}(\boldsymbol{k},\omega) = \mathbf{Q}^{L}(\boldsymbol{k},\omega) + \mathbf{Q}^{T}(\boldsymbol{k},\omega)$ and

$$\mathbf{Q}^{L} = \left(\tilde{\eta}k^2 + \frac{i\rho}{\omega}[\omega^2 - c^2k^2]\right)^{-1}\mathbf{P} = Q^{L}(\boldsymbol{k},\omega)\mathbf{P}, \tag{8}$$

$$\mathbf{Q}^{T} = (\eta k^2 + i\rho\omega)^{-1}(\mathbf{E}-\mathbf{P}) = Q^{T}(\boldsymbol{k},\omega)(\mathbf{E}-\mathbf{P}). \tag{9}$$

In the derivation of Eq. (7), we use the ideal gas equation of state, which applies to the MPC fluid. c is the isothermal velocity of sound, $\tilde{\eta} = \eta + \eta^{\mathrm{k}}/3$, and $\mathbf{E}$ denotes the unit matrix. Note that for angular-momentum conserving fluids $\tilde{\eta} = 4\eta/3$. Otherwise the same expressions (8) and (9) are obtained. $\mathbf{P}$ is a projection operator with the components $P_{\alpha\beta} = k_\alpha k_\beta/k^2$, $k = |\boldsymbol{k}|$, and projects a vector along the direction of $\boldsymbol{k}$. Hence, $\boldsymbol{v}(\boldsymbol{k},\omega) = \boldsymbol{v}^L(\boldsymbol{k},\omega) + \boldsymbol{v}^T(\boldsymbol{k},\omega)$ consists of a longitudinal part $\boldsymbol{v}^L$ and transverse part $\boldsymbol{v}^T$ with respect to $\boldsymbol{k}$, i.e., $\boldsymbol{v}(\boldsymbol{k},\omega)\cdot\boldsymbol{k} = v^L(\boldsymbol{k},\omega)k$ and $\boldsymbol{v}^T(\boldsymbol{k},\omega)\cdot\boldsymbol{k} = 0$. Fourier transformation with respect to ω yields

$$Q^T(\boldsymbol{k},t) = \frac{1}{\rho} e^{-\mu k^2 t}\Theta(t) \tag{10}$$

for the transverse part, where $\Theta(t)$ is Heaviside's function and $\mu = \eta/\rho$ denotes the kinematic viscosity. For the longitudinal contribution, we obtain the expression[65]

$$Q^L(\boldsymbol{k},t) = \frac{1}{\rho} e^{-k^2\tilde{\mu}t/2} \times \left[\cos(\Omega t) - \sqrt{\frac{k^2\tilde{\mu}^2}{4c^2 - k^2\tilde{\mu}^2}}\sin(\Omega t)\right]\Theta(t) \tag{11}$$

for $4c^2/(k^2\tilde{\mu}^2) > 1$, where $\Omega = k^2\tilde{\mu}\sqrt{4c^2/(k^2\tilde{\mu}^2) - 1}/2$ and $\tilde{\mu} = \tilde{\eta}/\rho$, and

$$Q^L(\boldsymbol{k},t) = \frac{1}{\rho} e^{-k^2\tilde{\mu}t/2} \times \left[\cosh(\Lambda t) - \sqrt{\frac{k^2\tilde{\mu}^2}{k^2\tilde{\mu}^2 - 4c^2}}\sinh(\Lambda t)\right]\Theta(t) \tag{12}$$

for $4c^2/(k^2\tilde{\mu}^2) < 1$, where $\Lambda = k^2\tilde{\mu}\sqrt{1 - 4c^2/(k^2\tilde{\mu}^2)}/2$.

For the sake of completeness, we present auto-correlation functions of the random velocity

$$\boldsymbol{v}^R(\boldsymbol{r},t) = \frac{1}{V}\iint \mathbf{Q}(\boldsymbol{r}-\boldsymbol{r}',t-t')\boldsymbol{f}^R(\boldsymbol{r}',t')\,d^3r'dt'. \tag{13}$$

In k-space, we obtain

$$\left\langle v_\alpha^R(\boldsymbol{k},t)v_\beta^R(\boldsymbol{k}',t')\right\rangle = \frac{k_BT}{V}\delta_{\boldsymbol{k},-\boldsymbol{k}'} \times \left[Q_{\alpha\beta}^T(\boldsymbol{k},t-t') + Q_{\alpha\beta}^L(\boldsymbol{k},t-t')\right], \tag{14}$$

with the matrix elements $Q_{\alpha\beta}^T(\boldsymbol{k},t) = Q^T(\boldsymbol{k},t)(\delta_{\alpha\beta} - P_{\alpha\beta})$ and $Q_{\alpha\beta}^L(\boldsymbol{k},t) = Q^L(\boldsymbol{k},t)P_{\alpha\beta}$. In real space the correlation functions become

$$\left\langle v_\alpha^R(\boldsymbol{r},t)v_\beta^R(\boldsymbol{r}',t')\right\rangle = \frac{k_BT}{V}\left[Q_{\alpha\beta}^T(\boldsymbol{r}-\boldsymbol{r}',t-t') + Q_{\alpha\beta}^L(\boldsymbol{r}-\boldsymbol{r}',t-t')\right]. \tag{15}$$

The expression for $\mathbf{Q}^T(\boldsymbol{r},t)$ is explicitly calculated in Ref. 86. The calculation of $\mathbf{Q}^L(\boldsymbol{r},t)$ is much more difficult due to the nonlinear dependence of $Q^L(\boldsymbol{k},t)$ on k^2. In both cases, we will perform the Fourier transformations numerically for the evaluation of the required correlation functions.

III. POLYMER DYNAMICS

A. Model

We consider a single linear flexible polymer embedded in a fluid. For the analytical description of the polymer dynamics, we adopt a mean-field model. Here, the polymer is considered to be a continuous space curve $\boldsymbol{r}(s,t)$, where s ($-L_p/2 \le s \le L_p/2$) is the contour coordinate along the chain of length L_p.[12,15,16,45] Its configurational "energy" is[7,16]

$$U_G = \frac{3k_BT}{2l}\int\left(\frac{\partial\boldsymbol{r}(s)}{\partial s}\right)^2 ds, \tag{16}$$

where l is the Kuhn segment length, T is the temperature, and k_B is Boltzmann's constant. No-slip boundary conditions are imposed, i.e., $\dot{\boldsymbol{r}}(s,t) = \boldsymbol{v}(\boldsymbol{r}(s,t),t)$, where $\boldsymbol{v}(\boldsymbol{r}(s,t),t)$ is the fluid flow field at the position $\boldsymbol{r}(s,t)$ of the polymer chain. The force density $\boldsymbol{f}^c$ in Eq. (2) is then

$$\boldsymbol{f}^c(\boldsymbol{r},t) = \int[\boldsymbol{F}(s',t) - \varrho\ddot{\boldsymbol{r}}(s',t)]\delta(\boldsymbol{r}-\boldsymbol{r}(s',t))\,ds' \tag{17}$$

with the inertial force $\varrho\ddot{\boldsymbol{r}}(s,t)$, and $\boldsymbol{F}(s) = -\delta U_G/\delta\boldsymbol{r}(s)$; ϱ is the linear polymer mass density. Hence, Eq. (7) yields the equation of motion for the polymer

$$\dot{\boldsymbol{r}}(s,t) = \boldsymbol{v}^R(\boldsymbol{r}(s,t),t) + \frac{1}{V}\iint\mathbf{Q}(\boldsymbol{r}(s,t)-\boldsymbol{r}(s',t'),t-t') \times[\boldsymbol{F}(s',t') - \varrho\ddot{\boldsymbol{r}}(s',t')]\,ds'dt'. \tag{18}$$

To solve the nonlinear equation, we apply Zimm's preaveraging approximation[2,7,12,16,54] and replace $\mathbf{Q}(\boldsymbol{r}(s,t)-\boldsymbol{r}(s',t'),t-t')$ by its average $\mathbf{Q}(s-s',t-t') = \langle\mathbf{Q}(\boldsymbol{r}(s,t)-\boldsymbol{r}(s',t'),t-t')\rangle = Q(s-s',t-t')\mathbf{E}$. Hence, Q is a function of the distance $s'-s$ along the polymer contour only. Similar, the preaveraging approximation implies that $\boldsymbol{v}^R(\boldsymbol{r}(s,t),t) \to \boldsymbol{v}^R(s,t)$, which is necessary to satisfy the fluctuation-dissipation relation.[87] Next, we perform the eigenfunction expansions

$$\boldsymbol{r}(s,t) = \sum_{n=0}^{\infty}\boldsymbol{\chi}_n(t)\varphi_n(s), \tag{19}$$

$$\boldsymbol{v}^R(s,t) = \sum_{n=0}^{\infty}\boldsymbol{v}_n^R(t)\varphi_n(s) \tag{20}$$

in terms of the eigenfunctions φ_n of the eigenvalue equation

$$\frac{3k_BT}{l}\frac{d^2}{ds^2}\varphi_n(s) + \xi_n\varphi_n(s) = 0 \tag{21}$$

with the eigenvalues ξ_n. The boundary conditions $d\varphi_n(s)/ds = 0$ for $s = \pm L_p/2$ lead to the eigenfunctions

$$\varphi_n(s) = \sqrt{\frac{2}{L}} \sin \frac{n\pi s}{L}, \text{ n odd}, \tag{22}$$

$$\varphi_n(s) = \sqrt{\frac{2}{L}} \cos \frac{n\pi s}{L}, \text{ n even}, \tag{23}$$

and the eigenvalues $\xi_n = 3\pi^2 k_B T n^2/(lL^2)$. In this representation, the matrix elements of the tensor $\mathbf{Q}(s - s', t)$ become

$$\mathbf{Q}_{nm}(t) = \frac{1}{V} \iint \varphi_n(s)\mathbf{Q}(s - s', t)\varphi_m(s')\, ds ds'. \tag{24}$$

The equations of motion for the normal-mode amplitudes are then given by

$$\dot{\boldsymbol{\chi}}_n(t) = \boldsymbol{v}_n^R(t) + \int \mathbf{Q}_{nn}(t - t')[-\xi_n \boldsymbol{\chi}_n(t') - \varrho \ddot{\boldsymbol{\chi}}_n(t')]dt'. \tag{25}$$

Here, the approximation $\mathbf{Q}_{nm} \approx \mathbf{Q}_{nn}\delta_{nm}$ has been used.[7,12,16] As pointed out in Ref. 12, a numerical calculation shows that the time-integrated matrix $\mathbf{Q}_{nm}^T$, i.e., the Oseen tensor is almost diagonal. As is evident from Refs. 30 and 47, off-diagonal elements lead to small quantitative differences between the solutions of the equations of motion with the full or diagonal tensor. However, an analytical solution is only possible for the diagonal tensor.

In the following, we will focus on the polymer center-of-mass dynamics, where the center-of-mass is defined as

$$\boldsymbol{r}_{cm}(t) = \frac{1}{L_p} \int_{-L_p/2}^{L_p/2} \boldsymbol{r}(s, t)\, ds = \boldsymbol{\chi}_0(t)\varphi_0 = \frac{1}{\sqrt{L_p}} \boldsymbol{\chi}_0(t) \tag{26}$$

and $\boldsymbol{v}_{cm}(t) = \dot{\boldsymbol{\chi}}_0(t)/\sqrt{L_p}$. Then, Fourier transformation with respect to time,

$$\dot{\boldsymbol{\chi}}_0(\omega) = \int \dot{\boldsymbol{\chi}}_0(t) e^{-i\omega t} dt, \tag{27}$$

of Eq. (25) yields, with $\xi_0 = 0$,

$$\dot{\boldsymbol{\chi}}_0(\omega) = \frac{\boldsymbol{v}_0^R(\omega)}{1 + i\omega\varrho Q_{00}(\omega)}. \tag{28}$$

B. Center-of-mass velocity correlation function

The center-of-mass velocity-correlation function can be written as

$$\langle \boldsymbol{v}_{cm}(t) \cdot \boldsymbol{v}_{cm}(0)\rangle = \frac{1}{(2\pi)^2 L_p} \iint \frac{\langle \boldsymbol{v}_0^R(\omega) \cdot \boldsymbol{v}_0^R(\omega')\rangle}{[1 + i\omega\varrho Q_{00}(\omega)][1 + i\omega\varrho Q_{00}(\omega')]} e^{i\omega t}\, d\omega d\omega' \tag{29}$$

by using Eqs. (26)–(28). The expression turns into

$$\langle \boldsymbol{v}_{cm}(t) \cdot \boldsymbol{v}_{cm}(0)\rangle = \frac{k_B T}{\pi V L_p} \int \frac{\sum_{\boldsymbol{k}} k^2 S(\boldsymbol{k})(2\eta|Q^T|^2 + \tilde{\eta}|Q^L|^2)}{[1 + i\omega\varrho Q_{00}(\omega)][1 - i\omega\varrho Q_{00}(-\omega)]} e^{i\omega t}\, d\omega \tag{30}$$

with the correlation function (A6) of Appendix A for the stochastic velocity, where [cf. Eq. (B5) of Appendix B]

$$Q_{00}(\omega) = \frac{1}{3V} \sum_{\boldsymbol{k}} S(\boldsymbol{k})[Q^L(k, \omega) + 2Q^T(k, \omega)] \tag{31}$$

and

$$S(\boldsymbol{k}) = \frac{1}{L_p} \iint \exp\left(-\frac{1}{6}\boldsymbol{k}^2 \langle [\boldsymbol{r}(s) - \boldsymbol{r}(s')]^2\rangle\right) ds ds' \tag{32}$$

is the polymer structure factor (A8).

As it turns out, our simulations yield an extremely weak dependence of the correlation function on the inertia term of the polymer for $t > 0$, i.e., on $i\omega\varrho Q_{00}$ in Eq. (30). Therefore, we neglect this term for our further considerations. Then, the center-of-mass correlation function becomes

$$\langle \boldsymbol{v}_{cm}(t) \cdot \boldsymbol{v}_{cm}(0)\rangle = \frac{k_B T}{V L_p} \sum_{\boldsymbol{k}} S(\boldsymbol{k})(2Q^T(\boldsymbol{k}, t) + Q^L(\boldsymbol{k}, t)), \tag{33}$$

after Fourier transformation with respect to ω. No closed expression can be provided for the right-hand side of this equation. However, the transverse part of the correlation function can be treated analytically for an infinitely large system.[55]

1. Transverse center-of-mass velocity correlation function

In the limit $L \to \infty$ of an infinitely large system, the transverse center-of-mass velocity correlation function [Eq. (33)] reads

$$\langle \boldsymbol{v}_{cm}^T(t) \cdot \boldsymbol{v}_{cm}^T(0)\rangle = \frac{k_B T}{\pi^2 L_p} \int S(k) Q^T(k, t) k^2 dk. \tag{34}$$

With Eqs. (10) and (32), integration yields

$$\langle \boldsymbol{v}_{cm}^T(t) \cdot \boldsymbol{v}_{cm}^T(0)\rangle = \frac{k_B T}{4\rho L_p^2 \sqrt{\pi^3}} \iint \left[\mu t + \frac{1}{6}\langle (\boldsymbol{r}(s) - \boldsymbol{r}(s'))^2\rangle\right]^{-3/2} ds ds'. \tag{35}$$

For a Gaussian polymer, where $\langle(\boldsymbol{r}(s)-\boldsymbol{r}(s'))^2\rangle = l|s-s'|$, the integrals can be evaluated, which implies

$$\left\langle \boldsymbol{v}_{cm}^T(t)\cdot\boldsymbol{v}_{cm}^T(0)\right\rangle = \frac{k_BT}{\rho\sqrt{\pi^3}R_g^3}\,\Xi\left(\mu t/R_g^2\right) \tag{36}$$

with the scaling function

$$\Xi(x) = (1/\sqrt{x} + 2[\sqrt{x}-\sqrt{x+1}]), \tag{37}$$

and the radius of gyration $R_g = \sqrt{lL/6}$. Hence, $\langle \boldsymbol{v}_{cm}^T(t)\cdot\boldsymbol{v}_{cm}^T(0)\rangle R_g^3$ is a universal function of $\mu t/R_g^2$. A similar expression has been derived in Ref. 55.

In the asymptotic limit $t \gg R_g^2/\mu$, the expression turns into

$$\left\langle \boldsymbol{v}_{cm}^T(t)\cdot\boldsymbol{v}_{cm}^T(0)\right\rangle = \frac{k_BT}{4\rho\sqrt{\pi^3}}\frac{1}{\sqrt{(\mu t)^3}}. \tag{38}$$

Thus, a long-time tail is obtained, which is independent of the polymer properties; it is solely determined by the fluid, as already shown in Refs. 54 and 55. In the opposite limit $t \ll R_g^2/\mu$, the correlation function becomes[55]

$$\left\langle \boldsymbol{v}_{cm}^T(t)\cdot\boldsymbol{v}_{cm}^T(0)\right\rangle = \frac{k_BT}{\rho R_g^2}\frac{1}{\sqrt{\pi^3\mu t}}. \tag{39}$$

This expression diverges in the limit $t \to 0$ and does not assume the equilibrium statistical mechanics value, i.e., the equipartition value of the kinetic energy. The reason is that we consider the over-damped polymer dynamics. Naturally, our approach only applies on times scales where polymer inertia effects are negligible.

The long-time tail (38) is solely determined by the fluid kinematic viscosity, whereas the velocity correlation function of a MPC particle also includes the particle's diffusion coefficient.[65] This is a consequence of the fact that the dynamic structure factor is replaced by the static structure factor. Hence, within the applied preaveraging approximation, we neglect any time dependence in the polymer segmental mean square displacement (MSD) with respect to the terms μt and $\tilde{\mu} t/2$, respectively, in the expression (33). This is certainly justified for the center-of-mass dynamics—the long-time segmental dynamics is equal to the center-of-mass dynamics—since the polymer center-of-mass diffusion coefficient is much small than the kinematic viscosity.

So far, we have considered Gaussian phantom polymers. As shown in Appendix C, the correlation function can also be calculated for a self-avoiding polymer in the limit $\mu t/R_g^2 \ll 1$, which yields the dependence

$$\left\langle \boldsymbol{v}_{cm}^T(t)\cdot\boldsymbol{v}_{cm}^T(0)\right\rangle \sim R_g^{-1/\nu}(\mu t)^{1/2\nu-3/2}, \tag{40}$$

where $\nu \approx 3/5$ is the (Flory) scaling exponent.[7]

2. Longitudinal center-of-mass velocity correlation function

For an infinite system, the longitudinal velocity correlation function is given by

$$\left\langle v_{cm}^L(t)v_{cm}^L(0)\right\rangle = \frac{k_BT}{2\pi^2L_p}\int S(k)Q^L(k,t)k^2dk, \tag{41}$$

when we use the correlation function (14). To find an analytical solution for this correlation function, we consider the limit $k\tilde{\mu}/c \ll 1$, i.e., small k values. This yields a satisfactory approximation for times $\tilde{\mu}k^2t \gg 1$, since for such long times the exponential factor in Q^L suppresses the contributions from large k-values in the integral. Then, Eq. (11) can be written as

$$Q^L(k,t) = \frac{1}{\rho}e^{-k^2\tilde{\mu}t/2}\cos(kct). \tag{42}$$

With the structure factor [Eq. (32)],

$$S(k) = \frac{2L_p}{k^2R_g^2}\left[1 - \frac{1}{R_g^2k^2} + \frac{1}{R_g^2k^2}e^{-k^2R_g^2}\right] \tag{43}$$

for Gaussian phantom polymers, Eq. (41) yields the correlation function

$$\left\langle v_{cm}^L(t)v_{cm}^L(0)\right\rangle = \frac{k_BT}{2\rho\pi^2R_g^4\sqrt{\tilde{\mu}t}}\left\{\sqrt{2\pi}\left[\left(R_g^2+\tilde{\mu}t\right)\exp\left(-\frac{c^2t}{2\tilde{\mu}}\right) - \sqrt{\tilde{\mu}t}\sqrt{2R_g^2+\tilde{\mu}t}\exp\left(-\frac{c^2t^2}{2\left(2R_g^2+\tilde{\mu}t\right)}\right)\right]\right.$$
$$\left. + \pi t\sqrt{\tilde{\mu}c^2t}\left[\mathrm{Erf}\left(\sqrt{\frac{c^2t}{2\tilde{\mu}}}\right) - \mathrm{Erf}\left(\sqrt{\frac{c^2t^2}{4R_g^2+2\tilde{\mu}t}}\right)\right]\right\}. \tag{44}$$

Here, Erf(x) is the error function.[88]

C. Diffusion coefficient

The center-of-mass diffusion coefficient is obtained by the Green-Kubo relation[7,87]

$$D = \frac{1}{3}\int_0^\infty \langle \boldsymbol{v}_{cm}(t')\cdot\boldsymbol{v}_{cm}(0)\rangle dt'. \tag{45}$$

The correlation function (33) is easily integrated. As is well known, sound is not contributing to the diffusion coefficient, because the integral over Q^L vanishes. The remaining transverse part yields the Zimm diffusion coefficient[7,12]

$$D_z = \frac{8k_BT}{3\sqrt{6\pi^3}\eta}\frac{1}{\sqrt{lL}} = \frac{4k_BT}{9\sqrt{\pi^3}\eta}\frac{1}{R_g}. \tag{46}$$

D. Mean square displacement

The polymer center-of-mass MSD $\Delta\boldsymbol{r}_{cm}^2(t) = \langle(\boldsymbol{r}_{cm}(t) - \boldsymbol{r}_{cm}(0))^2\rangle$ follows from Eq. (33) by the integral

$$\Delta \boldsymbol{r}_{cm}^2(t) = \int_0^t (t-t')\langle \boldsymbol{v}_{cm}(t') \cdot \boldsymbol{v}_{cm}(0)\rangle dt'. \quad (47)$$

This integral can easily be performed for the transverse correlation function (36), which yields

$$\Delta \boldsymbol{r}_{cm}^2(t) = 6D_z t \Upsilon\left(\mu t/R_g^2\right) \quad (48)$$

with the scaling function

$$\Upsilon(x) = 1 + x^{1/2} - \frac{2}{5x}[(x+1)^{5/2} - x^{5/2} - 1], \quad (49)$$

as already shown in Ref. 54. In the asymptotic limit of long times, the expression turns into[54,55]

$$\Delta \boldsymbol{r}_{cm}^2(t) = 6D_z\left(t - \frac{3}{4}\sqrt{\frac{R_g^2 t}{\mu}}\right). \quad (50)$$

Hence, the linear Einstein regime is reached slowly for $t\mu/R_g^2 \gg 1$.

For the sake of completeness and for comparison with simulation results, we also provide the well-known mean square displacement of a segment in the polymer center-of-mass reference frame[7,12,45]

$$\Delta \boldsymbol{r}_m^2(t) = \frac{2lL_p}{\pi^2}\sum_{n=1}^{\infty}\frac{1}{n^2}\left[1 - \exp\left(-\frac{tn^{3/2}}{\tau_z}\right)\right], \quad (51)$$

which follows from the Zimm model with a time-independent hydrodynamic tensor. τ_z is the Zimm relaxation time

$$\tau_z = \frac{6\sqrt{2}\eta}{\sqrt{\pi}k_BT}R_g^3. \quad (52)$$

The monomer dynamics will certainly depend on $\mathbf{Q}(s,t)$ [cf. Eq. (24)] at short times. However, the calculation of $\Delta \boldsymbol{r}_m^2$ requires the solutions of Eq. (25) for all modes, which will be discussed in a future article.

E. Discussion

Figure 1 displays analytical results of the normalized polymer center-of-mass velocity correlation function [Eq. (33)],

$$C_v(t) = C_v^T(t) + C_v^L(t) = \frac{m}{k_BT}\langle \boldsymbol{v}_{cm}(t) \cdot \boldsymbol{v}_{cm}(0)\rangle \quad (53)$$

with its transverse, C_v^T, and longitudinal, C_v^L, contributions according to Eqs. (36) and (41), in the asymptotic limit of a large system size. For the fluid parameters μ, $\tilde{\mu}$, ρ, and c, we choose values corresponding to the MPC fluid, which will be studied in Sec. IV, i.e., $\mu = 0.87\sqrt{k_BTa^2/m}$, $\tilde{\mu} = 0.89\sqrt{k_BTa^2/m}$, $\rho = 10m/a^3$, and $c/\sqrt{k_BT/m} = 1$ with the units of the MPC method.

There are various characteristic time scales for the fluid and polymer dynamics.

- The longitudinal velocity correlation function becomes negative above a polymer-length-dependent time τ_x.
- The time scale τ_c associated with sound propagation is given by the ratio of a characteristic polymer length scale and the velocity of sound. For a polymer coil, a suitable length scale is the radius of gyration, hence $\tau_c = R_g/c$.
- The viscous time τ_μ corresponds to the time of momentum diffusion over a radius of gyration, i.e., $\tau_\mu = R_g^2/\mu$.
- The longest polymer relaxation time is the end-to-end vector relaxation time $\tau_r \sim \eta R_g^3/(k_BT)$.

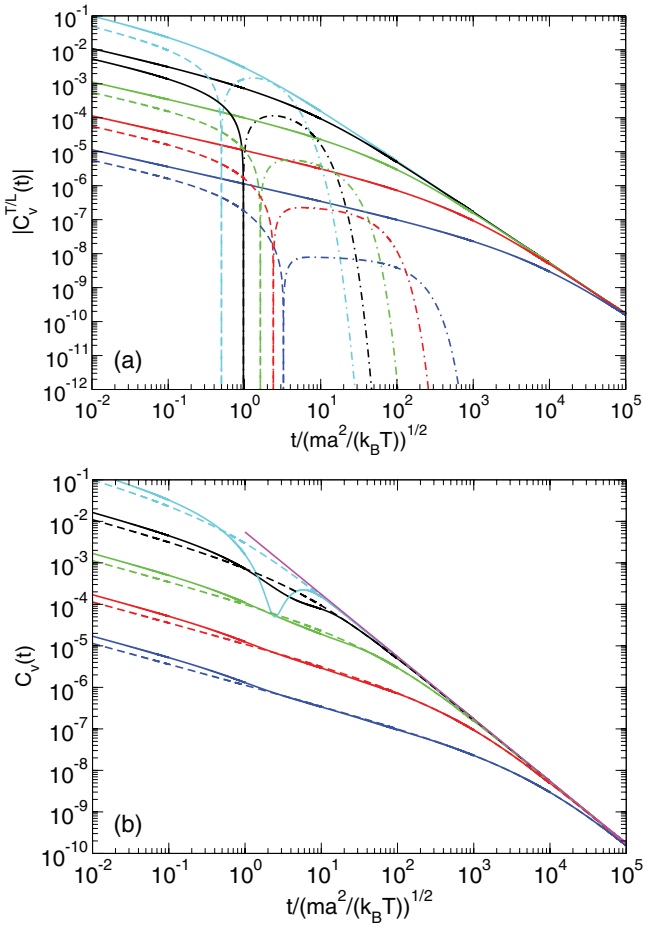

FIG. 1. Analytical center-of-mass velocity correlation functions $C_v = m\langle \boldsymbol{v}_{cm}(t) \cdot \boldsymbol{v}_{cm}(0)\rangle / k_BT$. (a) Transverse [Eq. (36)] (solid lines) and magnitudes of longitudinal [Eq. (41)] (dashed lines) correlation functions. The dashed-dotted lines represent negative parts. (b) Total correlation functions (solid lines) and the contributions of the transverse parts (dashed lines). The magenta line indicates the fluid long-time tail according to Eq. (38). The polymer lengths are $L_p/l = 10$, 10^2, 10^3, 10^4, and 10^5 (top to bottom).

For the lengths and viscosity of Fig. 1, the time τ_c approximately corresponds to the time where C_v^L increases strongly at the end of a plateau-like regime. Above this time, the correlation function C_v^L decays to zero very fast. A numerical fit yields a stretched exponential, i.e., $C_v^L \sim e^{-(t/t_0)^\zeta}$, with a length-dependent exponent $\zeta \geq 1$. The contribution of the longitudinal mode to the total correlation function decreases with increasing polymer length. This is also reflected in Fig. 1(b), which shows a comparison of total correlation functions and the corresponding transverse parts only. For all polymer lengths, we find a certain difference between the two quantities for $t/\hat{t} < 1$. In addition, shorter polymers exhibit a "sound dip" for somewhat larger times.

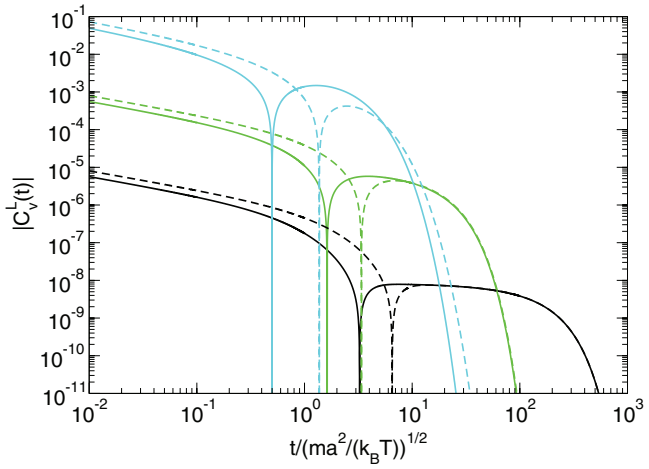

FIG. 2. Analytical longitudinal center-of-mass velocity correlation functions for the polymer lengths $L_p/l = 10$, 10^3, and 10^5 (top to bottom). The solid lines represent the full expression (41) and the dashed lines the approximation (44).

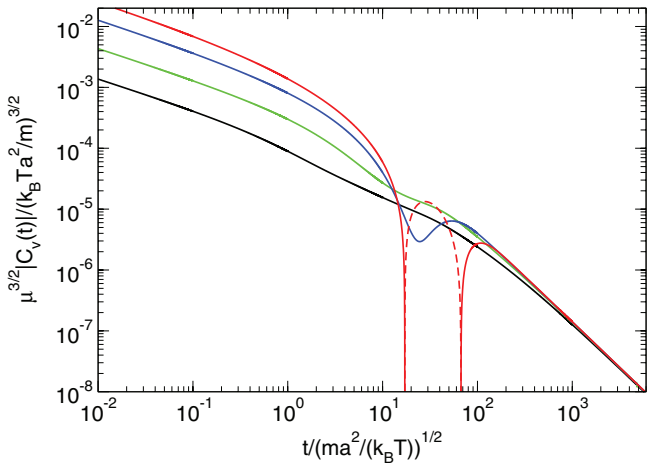

FIG. 3. Analytical center-of-mass velocity correlation functions of the polymer of length $L_p/l = 10^3$ and the collision time steps $h/\hat{t} = 0.05$ (red), 0.01 (blue), 0.03 (green), and 0.1 (black). These values correspond to the kinematic viscosities $\mu/\sqrt{k_BTa^2/m} = 16.4$, 8.2, 2.8, and 0.9.

Above τ_μ, the correlation functions become independent of the polymer properties, as discussed in Sec. III B 1. For $t \gg \tau_\mu$, the transverse velocity correlation functions approach the fluid asymptotic long-time tail.

The full expression (41) of the velocity-correlation function $C_v^L(t)$ is compared with the approximation (44) in Fig. 2. We obtain good agreement for polymer lengths $L_p/l > 200$ and long times. The magnitude of $C_v^L(t)$ in the "plateau-like" regime decreases as $|C_v^L| \sim R_g^{-3}$ with the radius of gyration of the polymer. The transverse contribution to the velocity correlation function decreases as $|C_v^T| \sim 1/R_g^2$. Thus, for polymers with $R_g^2/l^2 \gtrsim 100$, the total correlation function is determined by the transverse part only beyond the time τ_x, where the C_v^L becomes negative.

The analytical calculations [Eq. (39)] predict the dependence $C_v^T \sim 1/\sqrt{\mu t}$ of the transverse correlation function for $t \ll \tau_\mu$. Due to the presence of sound, C_v shows such a dependence for extremely long polymers only. Already for $L_p/l \lesssim 10^4$, we observe deviations from this prediction, and finite-size (polymer) properties determine the actual time dependence above the time τ_x.

Figure 3 illustrates the influence of the fluid viscosity on the polymer correlation function $C_v(t)$. Evidently, a larger viscosity implies a more pronounced sound effect. The presence or lack of longitudinal contributions to $C_v(t)$ depends on both, polymer length and viscosity.

Due to the fast decay of $C_v^L(t)$ for $t/\tau_c > 1$, sound yields no contribution to the center-of-mass mean square displacement (47) above τ_c. For longer polymers, the sound contribution is even negligible for $t/\tau_x \gtrsim 1$.

IV. SIMULATION MODELS

A. Polymer model

Similar to Sec. III, we consider a single linear flexible polymer. Two different polymer models are considered, a Gaussian phantom chain and a self-avoiding chain with excluded-volume interactions between non-bonded pairs of monomers.[25,64] For the Gaussian chain, the bond potential is[7,89]

$$U_G = \frac{3k_BT}{2l^2} \sum_{\lambda=1}^{N_m-1} (\boldsymbol{r}_{\lambda+1} - \boldsymbol{r}_\lambda)^2, \tag{54}$$

where $\boldsymbol{r}_\lambda(t)$ is the position of monomer λ ($\lambda = 1, \ldots, N_m$) and l is the root-mean-square bond length.

For the self-avoiding polymer, the bond potential is

$$U_{EV} = \frac{\kappa}{2} \sum_{\lambda=1}^{N_m-1} (|\boldsymbol{r}_{\lambda+1} - \boldsymbol{r}_\lambda| - l)^2, \tag{55}$$

where κ is the spring constant. Excluded-volume interactions are taken into account by the repulsive, shifted, and truncated Lennard-Jones potential

$$U_{LJ} = \begin{cases} 4\epsilon \left[\left(\frac{\sigma}{r}\right)^{12} - \left(\frac{\sigma}{r}\right)^6 + \frac{1}{4} \right] & \text{for } r > \sqrt[6]{2}\sigma \\ 0 & \text{otherwise,} \end{cases} \tag{56}$$

where the parameter σ characterizes the monomer size and ϵ the energy.[25,31] The dynamics of the monomers is determined by Newton's equation of motion, which are integrated by the velocity Verlet algorithm with the time step h_p.[90]

B. MPC fluid

The multiparticle collision dynamics fluid is composed of N point particles of mass m in a cubic periodic system of volume $V = L^3$, which interact with each other by a stochastic process.[62–64] The particle dynamics comprises alternating streaming and collision steps. In the streaming step, the particles advance ballistically for a time h, which we denote as collision time, i.e.,

$$\boldsymbol{r}_i(t+h) = \boldsymbol{r}_i(t) + h\boldsymbol{v}_i(t), \tag{57}$$

where $\boldsymbol{r}_i(t)$ and $\boldsymbol{v}_i(t)$ are the position and velocity of particle i ($i = 1, \ldots, N$). In the collision step, particles are sorted into cubic cells of side length a and their relative velocities, with

respect to the center-of-mass velocity of their cell, are rotated around a randomly oriented axis by a fixed angle α,

$$\boldsymbol{v}_i(t+h) = \boldsymbol{v}_i(t) + [\mathbf{R}(\alpha) - \mathbf{E}]\,[\boldsymbol{v}_i(t) - \boldsymbol{v}_{cm}(t)]\,. \quad (58)$$

$\mathbf{R}(\alpha)$ is the rotation matrix[64,91] and

$$\boldsymbol{v}_{cm}(t) = \frac{1}{N_c}\sum_{j=1}^{N_c} \boldsymbol{v}_j(t) \quad (59)$$

is the center-of-mass velocity of the particles in the cell of particle i, and N_c is the total number of solvent particles in that cell.[62–64] Despite discretization of space, Galilean invariance is reestablished by a random shift of the collision-cell lattice.[79] The algorithm preserves mass, momentum, and energy in a collision step, which leads to correlations between the particles and gives raise to hydrodynamic interactions. A local Maxwellian thermostat is used to maintain the temperature of the fluid at the desired value.[91] The fluid-polymer coupling is achieved by taking the monomers into account in the collision step.[25,64,92]

We implement our simulations on Graphics Processing Units (GPUs), which enhances the performance significantly over an equivalent simulation on a single CPU processor.[93] Thereby, we use a hybrid approach, where MPC is performed on the GPU and the molecular dynamics simulations of the polymers are performed on a CPU.

C. Simulation parameter

Simulation parameters for the various system sizes are listed in Tables I and II. Length and time are scaled by the collision-cell size a and $\hat{t} = \sqrt{ma^2/(k_BT)}$, respectively. The MPC rotation angle is chosen as $\alpha = 130^\circ$, and the mean number of fluid particles per collision cell is $\langle N_c\rangle = 10$. For the polymer, we set $l = \sigma = a$, $k_BT/\epsilon = 1$, and $M = m\langle N_c\rangle$. The spring constant κ is set to $\kappa = 100\,k_BT/l^2$. The molecular dynamics simulation time step is chosen as $h_p/\hat{t} = 2\times10^{-3}$.

V. SIMULATION RESULTS

We consider a wide range of polymer lengths. The actual values are summarized in Tables I and II for the Gaussian and self-avoiding polymers, respectively. Averages are taken over time and various initial conditions. We consider between 30 and 150 independent realizations of length $10^4 - 6\times10^5$ time units for a particular parameter set, where less but longer simulations are performed for the shorter polymers.

TABLE I. Simulation parameters and results for Gaussian phantom chains. N_m denotes the number of monomers, L is the length of the simulation box, R_g is the radius of gyration, and τ_r is the end-to-end vector relaxation time.

N_m	L/l	$h/\hat{t}$	R_g^2/l	$\tau_r/\hat{t}$
40	50	0.1	6.8	1300
80	40, 75, 140	0.1	13	3430
160	100	0.1	27	10 820
320	140	0.1	54	27 950
640	150	0.1	105	67 000
1280	140, 248	0.1	214	199 520
1280	248	0.02	211	1 112 940

TABLE II. Simulation parameters and results for self-avoiding polymers. N_m denotes the number of monomers, L is the length of the simulation box, R_g is the radius of gyration, and τ_r is the end-to-end vector relaxation time.

N_m	L/l	$h/\hat{t}$	R_g^2/l	$\tau_r/\hat{t}$
40	75	0.1	20	4800
80	120	0.1	47	15 600
160	160	0.1	110	50 000
320	140	0.1	250	168 000
640	140	0.1	525	527 000

A. Center-of-mass velocity-autocorrelation function

Simulation results for the polymer center-of-mass velocity correlation function (53) are shown in Fig. 4 for two collision time steps. At $t = 0$, the correlation functions assume

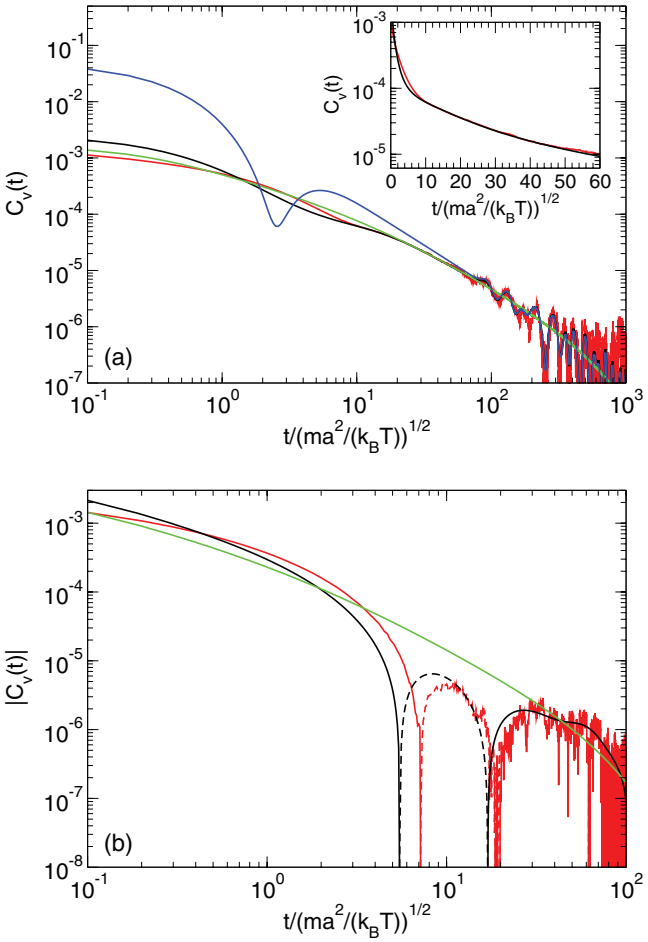

FIG. 4. Polymer center-of-mass velocity autocorrelation functions. (a) The polymer length is $N_m = 160$ and the collision time step $h/\hat{t} = 0.1$ ($\mu/\sqrt{k_BTa^2/m} = 0.87$). The inset shows the data in semilogarithmic representation. (b) The polymer length is $N_m = 80$ and $h/\hat{t} = 0.02$ ($\mu/\sqrt{k_BTa^2/m} = 4.12$). The negative parts of C_v are shown by dashed lines. The simulation results are displayed by red lines, the analytical results (33) by black lines, and the transverse contributions by green lines. The blue line in (a) indicates the correlation function of MPC particles.[65] The maximum mode numbers are (a) $n_m = 33$ and (b) $n_m = 25$ [cf. Eq. (60)].

the value $\langle \boldsymbol{v}_{cm}^2 \rangle = 3\, k_B T/(M N_m)$. After a very few MPC collisions, inertia effects disappear and the polymer dynamics is governed by hydrodynamic interactions. Correspondingly, the correlation functions reflect the theoretically predicted behavior and the theoretical expression describes the simulation result very well for $t/\hat{t} \gtrsim 10$. As discussed in Ref. 65, the lattice structure of the MPC method with its collision cells leads to a largest k-value, or smallest length scale, above hydrodynamic correlations disappear. Hence, we have to introduce an upper cut-off

$$k_m = \frac{2\pi n_m}{L} \tag{60}$$

in the calculation of the correlation function (33). The corresponding values n_m, which yield the best match between theory and simulations, are listed in the figure caption.

For short times, we observe deviations between the theoretical description and the simulation data, which are related to MPC specific aspects, and therefore cannot be captured by the fluctuating hydrodynamics approach. In any case, for the description of the equilibrium behavior at $t = 0$, polymer inertia has to be taken into account in order to obtain the proper equilibrium average of the center-of-mass kinetic energy.

Figure 4 confirms that the strength of the sound effect depends on the collision step size and increases with decreasing h, in agreement with the theoretical prediction presented in Fig. 3. For $t/\hat{t} > 100$, the polymer contribution to the correlation function disappears evidently [cf. Fig. 4(a)] and C_v is determined entirely by the MPC fluid. As discussed in Sec. III E, sound influences the correlation function on the time scale $t \approx \tau_c = R_g/c$. In Fig. 4, another sound effect is visible for $t \gtrsim L/c$ due to the periodic boundary conditions. The boundary conditions imply a reoccurrence of fluid sound waves after traversing the periodic system. This has been discussed in detail in Ref. 65. As expected, the sound modulations are also well described by the theoretical expression. For even longer times, the correlation functions decay exponentially.[65] The inset of Fig. 4(a) displays the simulation result in a semilogarithmic plot. Evidently, the correlation function is not decaying exponentially, neither for short times $t/\hat{t} \lesssim 5$ nor for longer times. In Ref. 92, an initial exponential decay is predicted, however, with no clear time-scale separation. A non-exponential decay was also obtained in Ref. 24 by Dissipative Dynamics Simulations (DPD).

The agreement between the analytical result and the simulation data over a wide range of time scales leads to an important conclusion on the influence of the finite simulation-box size on the velocity correlation function. Namely, the finite box size does not affect the correlation function for $t < L/c$, because the correlation function of the finite system is identical to that of an infinite system, as we have shown for a MPC fluid in Ref. 65. Only for $t \gtrsim L/c$, finite-size effects appear due to sound. In particular, for $t \gg L^2/[(2\pi)^2 \mu]$, only the value $k = 2\pi/L$ remains in the sum over $\boldsymbol{k}$ in (33), which implies an exponential decay of the correlation function.

Correlation functions for Gaussian and self-avoiding polymers of various polymer lengths are presented in Fig. 5. For self-avoiding polymers, we determine the respective structure factors from the simulations and use them in the evaluation of the analytical expression (33). The longitudinal contribution C_v^L is clearly visible for short polymers and gradually vanishes with increasing polymer length. In any case, the simulation data are very well described by the analytical prediction (33); even the finite-size corrections are reproduced at long times.

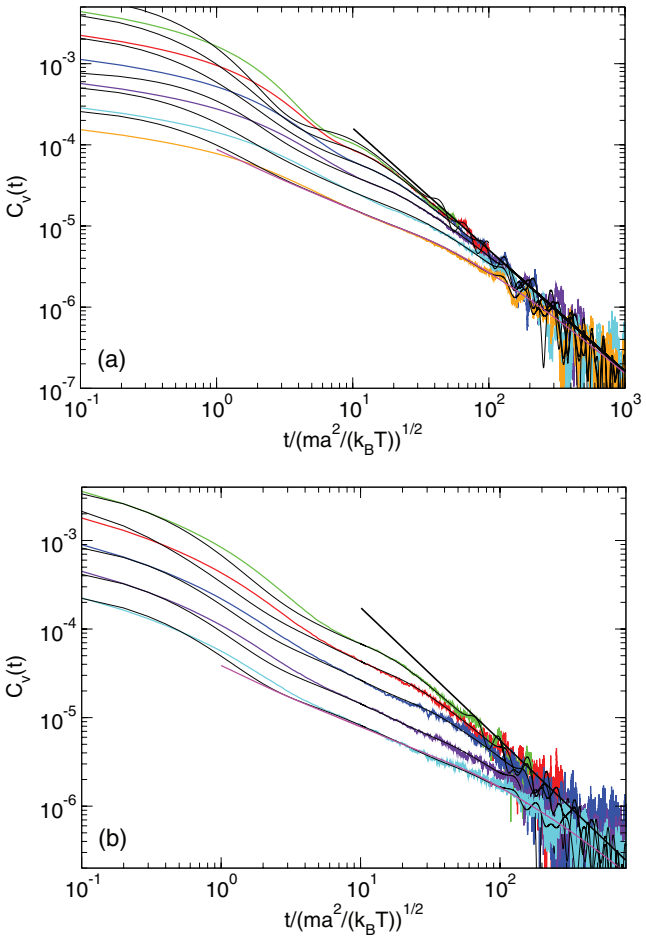

FIG. 5. (a) Simulation results for polymer center-of-mass velocity autocorrelation functions of Gaussian polymers of lengths $N_m = 40$, 80, 160, 320, 640, and 1280 (top to bottom), and (b) self-avoiding polymers of lengths $N_m = 40$, 80, 160, 320, and 640 (top to bottom). The black lines correspond to the analytical approximation (33) with the maximum mode numbers (a) $n_m = 15$, 25, 33, 50, and 40 for the two longer polymers, and (b) $n_m = 27$, 43, 57, and 50 for the longer ones, respectively. The straight lines indicate the long-time tail, and the magenta lines, for the longest polymers, the correlation functions for infinite systems.

Remarkably, the correlation functions for self-avoiding polymers are also very well described by the analytical theory above $t/\hat{t} \approx 7$, i.e., approximately for times where the longitudinal contribution becomes negative. The polymer properties are captured by the structure factor $S(k)$ in Eq. (33). At long times, the correlation functions are determined by small k values, i.e., by large-scale properties of the structure factor. On such scales, $S(\boldsymbol{k})$ is determined by the radius of gyration. Hence, the radius of gyration is the only polymer property, which appears in the correlation function at long times, for both, phantom and self-avoiding polymers. For shorter times, self-avoidance is reflected in the time dependence of $C_v^T(t)$. As discussed in Appendix C, we predict

an intermediate power-law regime with the time dependence $C_v \sim (\mu t)^{-3/10}$, in the limit of very long polymers.

Additionally, in Fig. 5, the correlation functions of the longest polymers are presented for $L \to \infty$. For Gaussian polymers, C_v can easily be obtained, since the structure factor is known (43). For self-avoiding polymers, in the calculation of the integrals (36) and (41), either the simulation result for the structure factor $S(k)$ can be used, or, as we do, the expression (43) is fitted to the simulation data, which yields the radius of gyration, and is used in the integral. As mentioned before, this applies because the long-time behavior of the velocity correlation function is determined by small k values. We then achieve an accurate descriptions on time scales $t > R_g^2/(4\pi^2\mu)$. Note that naturally the time $R_g^2/(4\pi^2\mu)$ has to be larger than the sound time τ_x. Independent of the applied (flexible) polymer model, the correlation function of the MPC fluid is assumed for $t \gg \tau_\mu$ in the asymptotic limit of large simulation boxes. As displayed in Fig. 5, the infinite-system-size correlation function describes the simulation data and the analytical result for the finite-size simulation box very well on the appropriate time scale.

The scaling properties of the center-of-mass velocity correlation function of Gaussian phantom polymers have been addressed in Ref. 24, where a characteristic time $\hat{\tau}_c$ was introduced to achieve universal long-time scaling, with the length dependence $\hat{\tau}_c \sim \sqrt{N_m}$. As noticed in Ref. 24 and is evident from our calculations, the length dependence of $\hat{\tau}_c$ is significantly different from $\tau_\mu \sim N_m$ [cf. Sec. III E], which is the appropriate characteristic time suggested by theory and confirmed by simulations. The inconsistence of the prediction $\hat{\tau}_c \sim \sqrt{N_m}$ has been discussed in Ref. 24, but has not been resolved. From our studies, we conclude that this scaling does not apply for polymers and is a consequence of the rather short chains considered in Ref. 24.

B. Diffusion coefficient

As pointed out in Sec. III C, the longitudinal center-of-mass velocity correlation function does not contribute to the diffusion coefficient. However, it is not *a priori* evident how quickly the integral over the sound contribution vanishes. To analyze how the asymptotic long-time limit is reached, we consider the time-dependent function

$$D(t) = \frac{1}{3}\int_0^t \langle \boldsymbol{v}_{cm}(t') \cdot \boldsymbol{v}_{cm}(0)\rangle dt', \tag{61}$$

which turns into the diffusion coefficient (45) in the limit $t \to \infty$.[59] Figure 6 shows simulation results for Gaussian polymers for various collision time steps, i.e., various viscosities. We present the product $\mu D(t)$, which is independent of viscosity for $t \to \infty$. The various curves approach the same asymptotic value within the accuracy of the simulations. How fast the limiting value is reached depends on the viscosity. Thereby, the trend is non-monotonic. A decreasing h leads to a faster approach of the asymptotic value, with a simultaneous decrease of the initial non-Brownian regime. The result for $h/\hat{t} = 0.02$ supports this idea. However, for even smaller h, the sound effect contributes substantially to the correlation function. $\mu D(t)$ even exceeds the asymptotic value in a wide

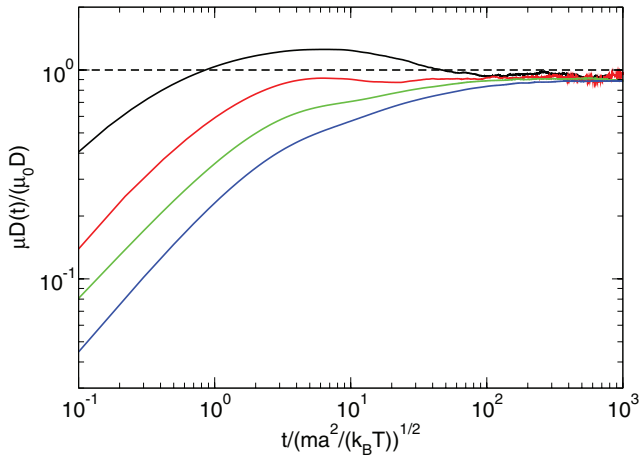

FIG. 6. Time integrals of the center-of-mass velocity autocorrelation functions (61) of Gaussian polymers of length $N_m = 80$ for the collision time steps step $h/\hat{t} = 0.1$ (blue), 0.05 (green), 0.02 (red), and 0.004 (black) (bottom to top). The corresponding kinematic viscosities are $\mu/\sqrt{k_BTa^2/m} = 0.87$, 1.67, 4.12, and 20.54, respectively. The product $\mu D(t)$ is scaled by the kinematic viscosity $\mu_0/\sqrt{k_BTa^2/m} = 0.87$ and the diffusion coefficient $D/\sqrt{k_BTa^2/m} = 2.2 \times 10^{-3}$ for the collision time step $h/\hat{t} = 0.1$.

time-range and assumes D_z at long times only. A similar effect has been found in backtracking of colloids in a MPC fluid.[59]

As is well known, finite system sizes severely affect the center-of-mass diffusion coefficient[21,24,25,67,94–98] as a consequence of the suppression of long-wavelength hydrodynamic modes by the periodic boundary conditions.[65] The self-diffusion coefficient D of a spherical particle of (hydrodynamic) radius R_h in a periodic system can be written as

$$D_L = D - \frac{k_BT}{6\pi\eta L}\left(2.837 - \frac{4\pi R_h^2}{3L^2}\right) \tag{62}$$

up to third order in the simulation box size L^{-1}.[97–99] D itself is related to the hydrodynamic radius R_h according to

$$D = \frac{k_BT}{6\pi\eta R_h} \tag{63}$$

for no-slip boundary conditions on the sphere surface. At large distance, we expect the flow field around a polymer to be similar to that around a spherical particle.[98] Therefore, Eq. (62) should also apply to polymer systems.

Typically, simulations for various box sizes are performed at constant ratio R_g/L (or R_h/L), and D is obtained by extrapolation to infinite box size. Here, we suggest an alternative and more efficient way to obtain the infinite system-size diffusion coefficient. As discussed, the polymer center-of-mass velocity correlation function can quantitatively be described by the theoretical expression (33) on time scales $t/\hat{t} \gtrsim 10$. Moreover, Fig. 7(a) illustrates that the correlation function is independent of system size on that time scale and for $t \le L/c$, where the latter shifts to infinity with increasing L. As pointed out before, finite-system-size effects are caused by the exponential decay of the correlation function at long times [cf. Fig. 7(a)].

To obtain the infinite-system-size correlation function, we suggest the following approach. A simulation of a moderately large system is performed and the finite-system-size cor-

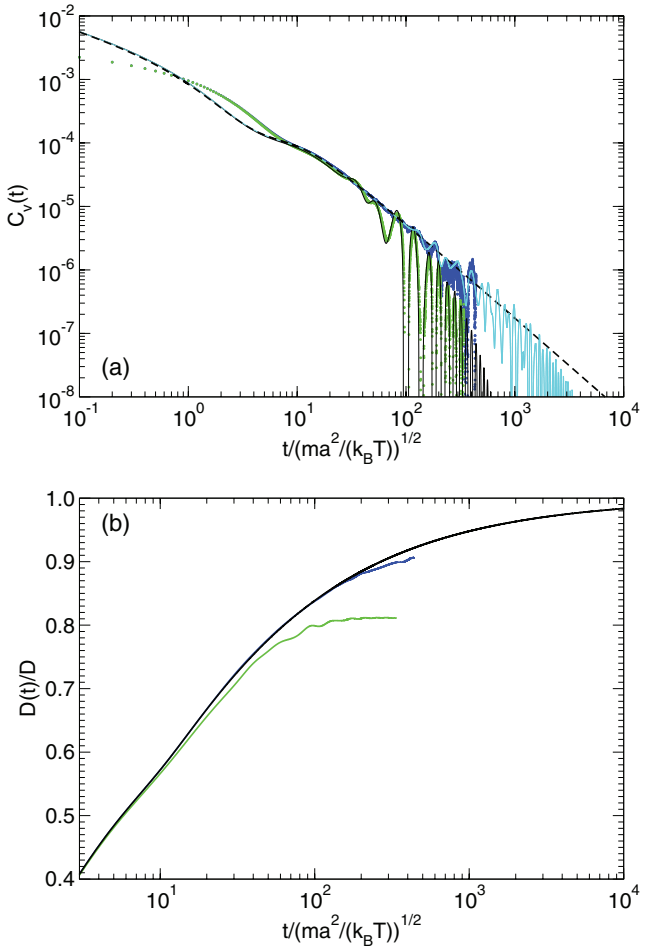

FIG. 7. (a) Center-of-mass velocity correlation functions of polymers of length $N_m = 80$. The lengths of the simulation boxes are $L/a = 40$ (green) and 140 (blue). At short times the two correlations are indistinguishable. The black and light blue lines are the corresponding theoretical results. The dashed line is the infinite system limit. (b) Integrated correlation functions. The same color code is applied as in (a). The black line follows as integral over the correlation function of the simulations up to $t/\hat{t} = 12$ and the theoretical correlation $C_v(t)$ beyond that time. The asymptotic value of the diffusion coefficient of the infinite system is $D/\sqrt{k_BTa^2/m} = 2.2 \times 10^{-3}$.

relation function is calculated. The theoretical velocity correlation function is determined using the structure factor (43) of the phantom polymer chain by fitting the theoretical expression to the simulation results in the vicinity of $kR_g \approx 1$. For phantom chains the theoretical expression describes the actual structure factor exactly. As discussed, in general, the long-time behavior of the velocity correlation function is determined by small k values only and we achieve an accurate descriptions of C_v on time scales $t > R_g^2/(4\pi^2\mu)$ even for self-avoiding polymers [cf. Fig. 5]. We replace then the (oscillating) tail of the finite-size simulation result by the analytical result and integrate the combined correlation function to obtain $D(t)$ and the asymptotic value D for $t \to \infty$.

An example for this procedure is provided in Fig. 7(b). The analytical result matches the simulation data for $L/a = 140$ above $t/\hat{t} \approx 12$ [cf. Fig. 7(a)]. From that time on, we replace the simulation result by the analytical correlation function and integrate the new combined function. The obtained result is shown as black line in Fig. 7(b). The asymptotic value of the diffusion coefficient of the infinite system is $D/\sqrt{k_BTa^2/m} = 2.2 \times 10^{-3}$, which is approximately 15% smaller than the diffusion coefficient $D_z = 2.5 \times 10^{-3}$ of the Zimm model [cf. Eq. (46)].

C. Mean square displacement

The dynamics of a polymer is further characterized by its center-of-mass MSD (50). The dynamics of the monomers is discussed in terms of their total average MSD,

$$\Delta \boldsymbol{r}_t^2 = \frac{1}{N_m} \sum_{\lambda=1}^{N_m} \langle (\boldsymbol{r}_\lambda(t) - \boldsymbol{r}_\lambda(0))^2 \rangle, \tag{64}$$

and their MSD in the center-of-mass reference frame

$$\Delta \boldsymbol{r}_m^2 = \frac{1}{N_m} \sum_{\lambda=1}^{N_m} \langle ([\boldsymbol{r}_\lambda(t) - \boldsymbol{r}_{cm}(t)] - [\boldsymbol{r}_\lambda(0) - \boldsymbol{r}_{cm}(0)])^2 \rangle. \tag{65}$$

1. Gaussian polymer

Figure 8 displays MSDs $\Delta \boldsymbol{r}_i^2(t)$, with $i \in \{m, t, cm\}$, of Gaussian polymers of various lengths. For a clear presentation, $\Delta \boldsymbol{r}_m^2(t)$ is shown separately in Fig. 8(b). The MSDs are scaled by twice the radius of gyration, the asymptotic long-time limit of $\Delta \boldsymbol{r}_m^2(t)$ predicted by the Zimm model [cf. Eq. (51)].[7,12,45] Time is scaled by the longest polymer relaxation time τ_r, extracted from the simulation data. The values are listed in Table I. For short polymers, we determine the relaxation time from the end-to-end vector correlation function, which decays exponentially for long times. For the longest polymer, the relaxation time is quite long and the calculation of a satisfactory precise value is extremely time consuming, even with a massively parallel simulation code. Therefore, we determine its relaxation time by a rescaling of the time such that $\Delta \boldsymbol{r}_m^2(t)$ superimposes with the corresponding MSDs of the shorter polymers for $t/\tau_r \gtrsim 10^{-3}$.

Figure 8 demonstrates that a universal behavior is obtained in the vicinity of $t/\tau_r \approx 1$ for all polymer lengths, in close agreement with the theoretical prediction of Eq. (51). Moreover, we observe a length-dependent (short) time regime, where $\Delta \boldsymbol{r}_m^2(t)$ displays a power-law behavior close to $t^{2/3}$, as predicted by the Zimm model for non-draining polymers [cf. Fig. 8(b)]. At short times, initial inertia effects play a role and for $t/\tau_r > 10^{-2}$ we observe a broad crossover regime to the asymptotic plateau value. Hence, much longer polymers are required to observe Zimm behavior over several orders of magnitude in the MSDs. The MSDs $\Delta \boldsymbol{r}_t^2(t)$ seem to follow the time dependence $t^{2/3}$ over a wider time range. However, this is a coincidence, because the crossover effect in the displacements $\Delta \boldsymbol{r}_m^2(t)$ is (partially) compensated by the center-of-mass MSDs.

The center-of-mass MSD approaches the linear dependence rather late. Only for $t/\tau_r \geq 1$, the free diffusion limit is reached for the collision time step $h/\hat{t} = 0.1$. For the smaller value $h/\hat{t} = 0.02$, the asymptotic limit is reached significantly earlier ($t/\tau_r \approx 10^{-3}$). According to the discussion of the dependence of $D(t)$ on the collision time step [cf. Fig. 6], this is a

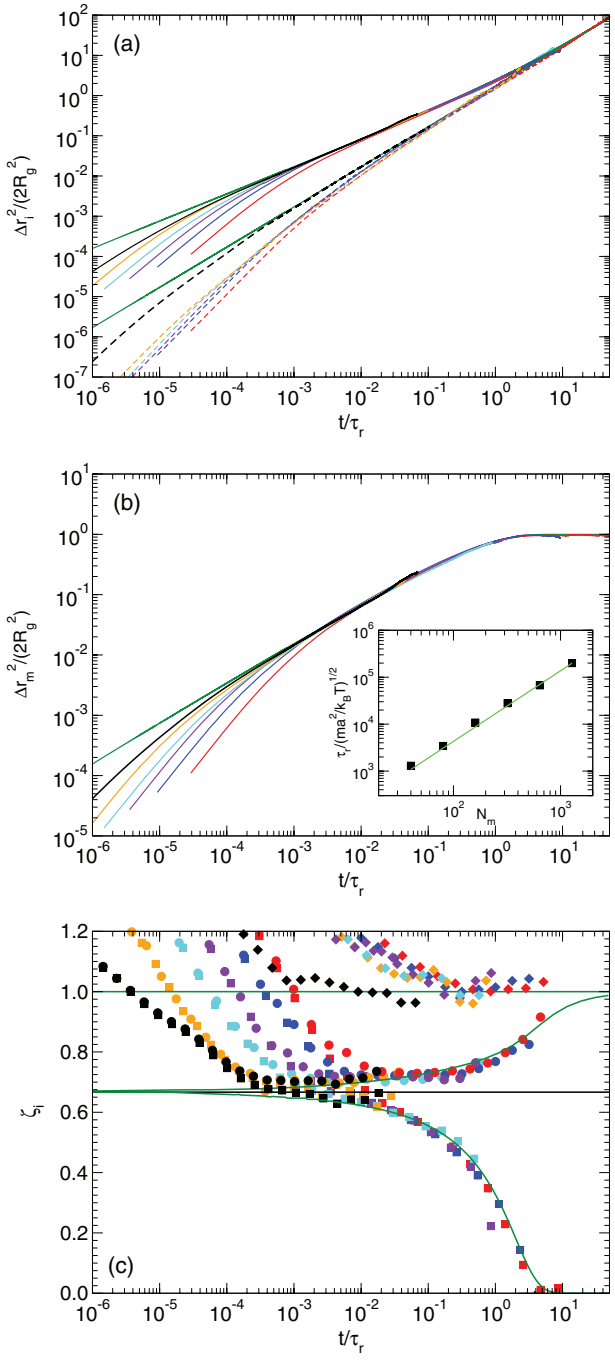

FIG. 8. (a) Means quare displacements of monomers $\Delta \boldsymbol{r}_i^2$ (solid lines) and of polymer centers-of-mass $\Delta \boldsymbol{r}_{cm}^2$ (dashed-dotted lines) for Gaussian polymers. (b) Monomer MSDs in the center-of-mass reference frame $\Delta \boldsymbol{r}_m^2$. (c) Local slopes [Eq. (66)] of the MSDs of (a) and (b): $\zeta_m(t)$ (squares), ζ_{cm} (diamonds), and ζ_t (bullets). The polymer lengths are $N_m = 80$ (red), 160 (blue), 320 (purple), 640 (light-blue), 1280 (with $h/\hat{t} = 0.1$) (orange), and 1280 (with $h\hat{t} = 0.02$) (black). The dark-green curves are theoretical results following from Eqs. (50)–(52). Inset in (b): Polymer-length dependence of the relaxation times. The solid line shows the power-law $\tau_r \sim N_m^{3/2}$.

coincidence due to cancellation of sound effects. The slow approach of the asymptotic long-time limit was already pointed out in Ref. 54. The inset in Fig. 8(b) shows the length dependence of the relaxation time. The values are consistent with the scaling relation $\tau_r \sim N_m^{3/2}$ of the Zimm model.[7]

Figure 8(c) presents the local slopes ζ_i of the MSDs of Figs. 8(a) and 8(b), which are calculated according to[45]

$$\zeta_i(t) = \frac{d[\log \Delta \boldsymbol{r}_i^2(t)]}{d \log t}. \tag{66}$$

Again, we find a small time window, where $\zeta_m \approx \zeta_t \approx 2/3$, particularly for longer polymers. For $t/\tau_r > 10^{-2}$, ζ_m decreases to zero, thereby following closely the dependence predicted by the Zimm approach. Similar, the slopes ζ_t follow the Zimm prediction above a polymer-length dependent time-ratio t/τ_r.

2. Self-avoiding polymer

The various MSDs for self-avoiding polymers are displayed in Fig. 9. Again, we extract the relaxation times of the two shortest polymers from the end-to-end vector correlation functions. The times of the longer polymers are obtained by matching the dependence of $\Delta \boldsymbol{r}_m^2(t)$ for $t/\tau_r \gtrsim 10^{-3}$. The corresponding relaxation times are listed in Table II and

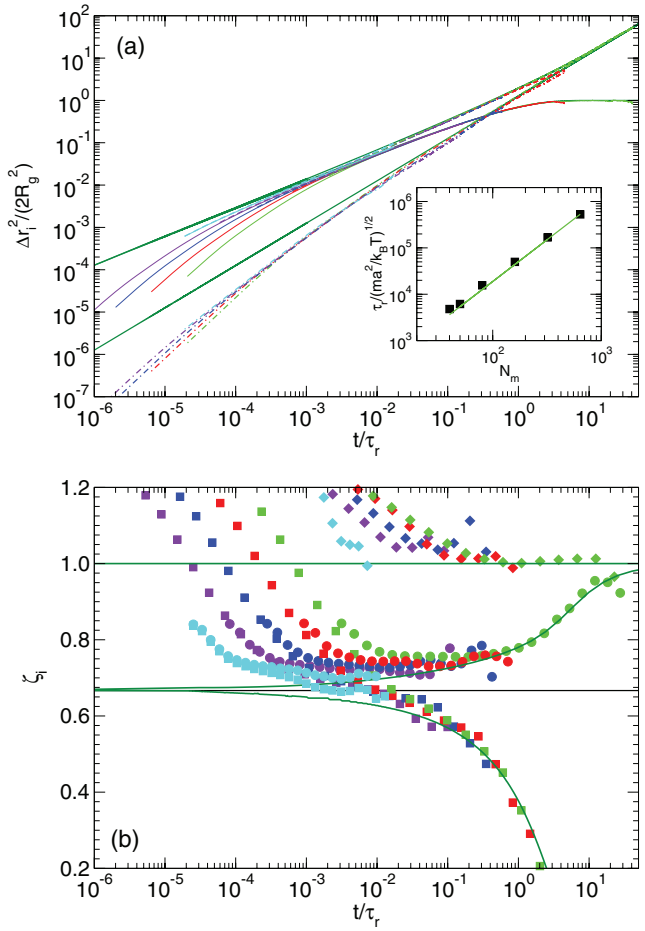

FIG. 9. (a) Mean square displacements of self-avoiding polymers: Monomer MSDs in the center-of-mass reference frame $\Delta \boldsymbol{r}_m^2$ (solid lines), total monomer MSDs $\Delta \boldsymbol{r}_i^2$ (dashed lines), and center-of mass MSDs $\Delta \boldsymbol{r}_{cm}^2$ (dashed-dotted lines). The polymer lengths are $N_m = 40$ (green), 80 (red), 160 (blue), 320 (purple), and 640 (light-blue). The dark-green curves are theoretical results following from Eqs. (50)–(52). (Inset) Polymer-length dependence of the relaxation times. The solid line shows the power-law $\tau_r \sim N_m^{2\nu}$, with $\nu = 0.6$. (b) Local slopes [Eq. (66)] of the MSDs of (a): $\zeta_m(t)$ (squares), ζ_{cm} (diamonds), and ζ_t (bullets).

displayed in the inset of Fig. 9(a). The length dependence follows the theoretical prediction $\tau_r \sim N_m^{3\nu}$, with $\nu \approx 0.6$.[7]

The $\Delta \boldsymbol{r}_m^2(t)$ indeed seem to show universal behavior in the vicinity of $t/\tau_r \approx 1$, a behavior which extends to shorter t/τ_r with increasing polymer length. The individual curves qualitatively follow the theoretical prediction (51). Since this expression does not apply to self-avoiding polymers in general,[7] we adjusted the time scale such that the theoretical curve quantitatively matches the simulation data in the vicinity of $t/\tau_r \approx 1$. This implies a shift of the theoretical curve along the (logarithmic) t/τ_r axis by a factor 1.35. As for the Gaussian polymer, we obtain a (short) scaling regime over which $\zeta_m \approx 2/3$ (see also Fig. 9(b)). Much longer polymers are required to see Zimm behavior over a larger time window. Figure 9 suggests that the slopes ζ_t for $\Delta \boldsymbol{r}_t^2(t)$ are nearly constant over a certain time range, but they are somewhat larger than the Zimm value 2/3. The slopes ζ_m are rather similar for $t/\tau_r \gtrsim 10^{-3}$, where the actual shortest time depends on polymer length, and follow qualitative the prediction of the Zimm model. Similar to the Gaussian polymer, the center-of-mass MSDs reach the asymptotic linear regime for $t/\tau_r \gtrsim 1$ only. We observe near quantitative agreement with the "shifted" theoretical curves.

VI. SUMMARY AND CONCLUSIONS

We have investigated the influence of time-dependent hydrodynamic correlations on the dynamical properties of a polymer in dilute solution. Particularly, the properties of compressible fluids have been addressed. Results of both analytical calculations and coarse-grained mesoscale hydrodynamic simulations are presented and compared. In general, the linearized Landau-Lifshitz Navier-Stokes equations, adapted to the SRD version of the MPC algorithm, describe the simulation results very well above a minimal length scale determined by the collision lattice of MPC.

As already obtained in Refs. 54 and 55 for incompressible fluids and Gaussian phantom chains, the transverse center-of-mass velocity correlation function exhibits a distinct dependence on the polymer properties on time scales $t/\tau_\mu < 1$, where $\tau_\mu = R_g^2/\mu$. We extended the theoretical calculations to self-avoiding polymers and find the general dependence $C_v^T(t) \sim (\mu t)^{1/2\nu-3/2}$ on the scaling exponent ν. For longer times, the correlation function is solely determined by fluid properties and exhibits the long-time tail, which decays as $(\mu t)^{-3/2}$ in three-dimensional space.

Fluid compressibility, which implies a finite sound velocity c, influences the correlation function on time scales comparable to $\tau_c = R_g/c$. Thereby, the sound effect is stronger for higher viscosities and may lead to partially negative correlation functions, resembling viscoelastic behavior. In general, the sound effect decreases with increasing polymer length. For time scales longer than τ_μ, the sound correlation function decreases in a stretched exponential manner. Hence, the asymptotic long-time behavior is determined by vorticity. Specifically, for Gaussian polymers, the vorticity correlation function is a universal function of $\mu t/R_g^2$, in contrast to various other proposed dependencies.[24,25]

Based on our analytical considerations, we propose a way to overcome the problematic in the calculation of the diffusion coefficient of finite-size periodic systems. To obtain the polymer center-of-mass diffusion coefficient in the limit of large system sizes, we suggest to amend its numerically determined velocity correlation function by the analytically derived expression on long time scales, where the dynamics is governed by fluid correlations only. This should be possible for all kinds of polymers, since the long-time dynamics is governed by small k values, i.e., length scales larger than the radius of gyration. The concept should also apply to other dilute systems such as colloids, since their long-time dynamics should also be determined by fluid correlations only.

Finally, we considered the mean square displacements of monomers and the polymer center of mass, for both Gaussian and self-avoiding polymers. As expected, the Gaussian polymers exhibit qualitative and quantitative agreement in their displacements with the prediction of the Zimm model above a certain time scale. We find the power-law behavior $t^{2/3}$ for $\Delta \boldsymbol{r}_m^2$ over a length-dependent short time window only. However, $\Delta \boldsymbol{r}_m^2$ closely follows the theoretical prediction for longer times. Similar features are displayed by self-avoiding polymers. In both cases, we obtain relaxation times, which exhibit the predicted length dependence $\tau_r \sim N_m^{3\nu}$, with $\nu = 1/2$ and $\nu \approx 3/5$ for Gaussian and self-avoiding polymers, respectively.

We consider the studies of the polymer mean square displacements as benchmark for studies of more concentrated systems. In the latter systems, screening effects appear for concentrations exceeding the overlap concentration. Then, the polymer MSDs should reflect the modified behavior. Theoretical predictions suggest that the MSD should exhibit Rouse rather then Zimm behavior above a certain time scale.[7] Our studies show that the different time scales and crossovers have to be considered very carefully in order to extract the correct scaling-laws in semidilute systems—both in simulations and experiments.

ACKNOWLEDGMENTS

Financial support by the German Research Foundation (DFG) within SFB TR6 and the European Union through FP7-Infrastructures ESMI (Grant No. 262348) is gratefully acknowledged. We are grateful to the Jülich Supercomputer Centre (JSC) for allocation of a CPU-time grant.

APPENDIX A: RANDOM FLUID VELOCITY CORRELATION FUNCTION

The zeroth-mode random velocity $\boldsymbol{v}_0^R(t)$ (20) can be expressed as

$$\boldsymbol{v}_0^R(t) = \int \varphi_0(s) \boldsymbol{v}^R(s,t)\, ds = \frac{1}{\sqrt{L_p}} \int \boldsymbol{v}^R(s,t)\, ds, \quad \text{(A1)}$$

and correspondingly

$$\boldsymbol{v}_0^R(\omega) = \frac{1}{\sqrt{L_p}} \int \boldsymbol{v}^R(s,\omega)\, ds. \quad \text{(A2)}$$

With the Fourier representation (5),

$$\boldsymbol{v}^R(\boldsymbol{r},\omega) = \sum_{\boldsymbol{k}} \boldsymbol{v}^R(\boldsymbol{k},\omega) e^{-i\boldsymbol{k}\boldsymbol{r}}, \tag{A3}$$

we obtain the velocity correlation function

$$\left\langle \boldsymbol{v}_0^R(\omega)\cdot\boldsymbol{v}_0^R(\omega')\right\rangle = \frac{1}{L_p}\sum_{\boldsymbol{k},\boldsymbol{k}'}\iint \langle e^{-i\boldsymbol{k}\boldsymbol{r}(s)} e^{-i\boldsymbol{k}'\boldsymbol{r}(s')}\rangle \times \langle \boldsymbol{v}^R(\boldsymbol{k},\omega)\cdot\boldsymbol{v}^R(\boldsymbol{k}',\omega')\rangle\, ds ds'. \tag{A4}$$

The stress-tensor correlation functions (3) yield

$$\left\langle \boldsymbol{v}^R(\boldsymbol{k},\omega)\cdot\boldsymbol{v}^R(\boldsymbol{k}',\omega')\right\rangle = \frac{4\pi k_B T}{V} k^2 \delta(\omega+\omega')\delta_{\boldsymbol{k},-\boldsymbol{k}'} \times (2\eta|Q^T(\boldsymbol{k},\omega)|^2 + \tilde{\eta}|Q^L(\boldsymbol{k},\omega)|^2). \tag{A5}$$

The factor two in front of $|Q^T(\boldsymbol{k},\omega)|^2$ reflects the two transverse components of vorticity. Hence,

$$\left\langle \boldsymbol{v}_0^R(\omega)\cdot\boldsymbol{v}_0^R(\omega')\right\rangle = \frac{4\pi k_B T}{V}\delta(\omega+\omega') \times \sum_{\boldsymbol{k}} k^2 S(\boldsymbol{k})(2\eta|Q^T(\boldsymbol{k},\omega)|^2 + \tilde{\eta}|Q^L(\boldsymbol{k},\omega)|^2), \tag{A6}$$

where S is the polymer structure factor

$$S(\boldsymbol{k}) = \frac{1}{L_p}\iint \langle e^{-i\boldsymbol{k}[\boldsymbol{r}(s)-\boldsymbol{r}(s')]}\rangle\, ds ds'. \tag{A7}$$

Due to the Gaussian nature of the polymer model, S is given by

$$S(\boldsymbol{k}) = \frac{1}{L_p}\iint \exp\left(-\frac{1}{6}\boldsymbol{k}^2\left\langle[\boldsymbol{r}(s)-\boldsymbol{r}(s')]^2\right\rangle\right) ds ds'. \tag{A8}$$

APPENDIX B: HYDRODYNAMIC TENSOR

In Fourier representation, the hydrodynamic tensor $\mathbf{Q}(\boldsymbol{r}-\boldsymbol{r}',t)$ reads

$$\mathbf{Q}(\boldsymbol{r}-\boldsymbol{r}',t) = \sum_{\boldsymbol{k}} e^{-i\boldsymbol{k}(\boldsymbol{r}-\boldsymbol{r}')}\mathbf{Q}(\boldsymbol{k},t) \tag{B1}$$

with $\mathbf{Q}(\boldsymbol{k},t) = Q^L(k,t)\mathbf{P} + Q^T(k,t)(\mathbf{E}-\mathbf{P})$; Q^T and Q^L are defined in Eqs. (10)–(12). $\mathbf{P}$ is the projection operator (8). Preaveraging yields

$$\langle \mathbf{Q}(\boldsymbol{r}-\boldsymbol{r}',t)\rangle = \sum_{\boldsymbol{k}}\langle e^{-i\boldsymbol{k}(\boldsymbol{r}-\boldsymbol{r}')}\rangle\mathbf{Q}(\boldsymbol{k},t) = \sum_{\boldsymbol{k}}\exp\left(-\frac{1}{6}\boldsymbol{k}^2\langle[\boldsymbol{r}-\boldsymbol{r}']^2\rangle\right)\mathbf{Q}(\boldsymbol{k},t). \tag{B2}$$

The exponential function as well as $Q^T(\boldsymbol{k},\omega)$ and $Q^L(\boldsymbol{k},\omega)$ depend on the magnitude of $\boldsymbol{k}$ only. Hence, all off-diagonal components of $\langle\mathbf{Q}(\boldsymbol{r}-\boldsymbol{r}',t)\rangle$ are zero within the preaveraging approximation. Moreover, our systems are homogeneous and isotropic. Thus, we obtain $\langle\mathbf{Q}(\boldsymbol{r}-\boldsymbol{r}',t)\rangle = Q(s-s',t)\mathbf{E}$, where

$$Q(s-s',t) = \frac{1}{3}\sum_{\boldsymbol{k}}\exp\left(-\frac{1}{6}\boldsymbol{k}^2\langle[\boldsymbol{r}(s)-\boldsymbol{r}(s')]^2\rangle\right) \times [Q^L(k,t)+2Q^T(k,t)]. \tag{B3}$$

In Fourier space, the zeroth-mode tensor component $Q_{00}(\omega)$ is related to $Q(s-s',\omega)$ according to

$$Q_{00}(\omega) = \frac{1}{VL_p}\iint Q(s-s',\omega)\, ds ds'. \tag{B4}$$

Inserting the Fourier transform of Eq. (B3) leads to

$$Q_{00}(\omega) = \frac{1}{3V}\sum_{\boldsymbol{k}} S(\boldsymbol{k})[Q^L(k,\omega)+2Q^T(k,\omega)]. \tag{B5}$$

APPENDIX C: CENTER-OF-MASS VELOCITY CORRELATION FUNCTION: SELF-AVOIDING POLYMER

The transverse center-of-mass velocity correlation function (35) can also be evaluated for a self-avoiding polymer in the limit $\mu t/R_g^2 \ll 1$. Note that Eq. (35) applies as long as the underlaying stochastic process is Gaussian (cf. Appendix A). Assuming self-similar polymer conformations, the second moment of the $\langle(\boldsymbol{r}(s)-\boldsymbol{r}(s'))^2\rangle$ can be written as[7]

$$\langle(\boldsymbol{r}(s)-\boldsymbol{r}(s'))^2\rangle = l^2\left(\frac{s-s'}{l}\right)^{2\nu} \tag{C1}$$

with the scaling exponent $\nu = 1/2$ for a phantom polymer and $\nu = 3/5$ for a self-avoiding polymer. Then, the correlation function becomes

$$\left\langle \boldsymbol{v}_{cm}^T(t)\cdot\boldsymbol{v}_{cm}^T(0)\right\rangle = \frac{k_B T}{2\rho\sqrt{(\pi\mu t)^3}} \times \int_0^1 \frac{1-x}{\left[1+R_g^2 x^{2\nu}/(\mu t)\right]^{3/2}} dx. \tag{C2}$$

Here, we introduce the more general radius of gyration $R_g = l(L_p/l)^\nu/\sqrt{6}$. By substitution, the integral turns into

$$\left\langle \boldsymbol{v}_{cm}^T(t)\cdot\boldsymbol{v}_{cm}^T(0)\right\rangle = \frac{k_B T}{2\rho\sqrt{\pi^3(R_g^2)^{1/\nu}}}(\mu t)^{1/2\nu-3/2} \times \int_0^\infty \frac{1}{[1+x^{2\nu}]^{3/2}} dx. \tag{C3}$$

For $\nu = 1/2$, the expression reduces to Eq. (39). For a self-avoiding polymer with $\nu = 3/5$, we find the time dependence

$$\left\langle \boldsymbol{v}_{cm}^T(t)\cdot\boldsymbol{v}_{cm}^T(0)\right\rangle \sim (\mu t)^{-3/10}. \tag{C4}$$

[1] J. G. Kirkwood and J. Riseman, J. Chem. Phys. **16**, 565 (1948).
[2] B. H. Zimm, J. Chem. Phys. **24**, 269 (1956).
[3] M. Fixman, J. Chem. Phys. **42**, 3831 (1965).
[4] H. Yamakawa, *Modern Theory of Polymer Solutions* (Harper & Row, New York, 1971).
[5] M. Bixon, Ann. Rev. Phys. Chem. **27**, 65 (1976).
[6] S. F. Edwards and M. Muthukumar, Macromolecules **17**, 586 (1984).

[7]M. Doi and S. F. Edwards, *The Theory of Polymer Dynamics* (Clarendon Press, Oxford, 1986).
[8]M. Fixman, Macromolecules **14**, 1710 (1981).
[9]S. R. Aragón and R. Pecora, Macromolecules **18**, 1868 (1985).
[10]R. B. Bird, C. F. Curtiss, R. C. Armstrong, and O. Hassager, *Dynamics of Polymer Liquids* (John Wiley & Sons, New York, 1987), Vol. 2.
[11]J. des Cloizeaux and G. Jannink, *Polymers in Solution: Their Modelling and Structure* (Clarendon Press, Oxford, 1990).
[12]L. Harnau, R. G. Winkler, and P. Reineker, J. Chem. Phys. **104**, 6355 (1996).
[13]H. C. Öttinger, *Stochastic Processes in Polymeric Fluids* (Springer, Berlin, 1996).
[14]K. Kroy and E. Frey, Phys. Rev. E **55**, 3092 (1997).
[15]R. G. Winkler, Phys. Rev. Lett. **97**, 128301 (2006).
[16]R. G. Winkler, J. Chem. Phys. **133**, 164905 (2010).
[17]J. Garcia de la Torre, A. Jimenez, and J. J. Freire, Macromolecules **15**, 148 (1982).
[18]C. Pierleoni and J.-P. Ryckaert, Phys. Rev. Lett. **66**, 2992 (1991).
[19]B. Dünweg and K. Kremer, Phys. Rev. Lett. **66**, 2996 (1991).
[20]C. Aust, M. Kröger, and S. Hess, Macromolecules **32**, 5660 (1999).
[21]N. A. Spenley, Europhys. Lett. **49**, 534 (2000).
[22]P. Ahlrichs, R. Everaers, and B. Dünweg, Phys. Rev. E **64**, 040501 (2001).
[23]R. M. Jendrejack, J. J. de Pablo, and M. D. Graham, J. Chem. Phys. **116**, 7752 (2002).
[24]C. P. Lowe, A. F. Bakker, and M. W. Dreischor, Europhys. Lett. **67**, 397 (2004).
[25]K. Mussawisade, M. Ripoll, R. G. Winkler, and G. Gompper, J. Chem. Phys. **123**, 144905 (2005).
[26]O. B. Usta, A. J. C. Ladd, and J. E. Butler, J. Chem. Phys. **122**, 094902 (2005).
[27]J. E. Butler and E. S. G. Shaqfeh, J. Chem. Phys. **122**, 014901 (2005).
[28]W. Jiang, J. Huang, Y. Wang, and M. Laradji, J. Chem. Phys. **126**, 044901 (2007).
[29]S. Frank and R. G. Winkler, EPL **83**, 38004 (2008).
[30]M. Hinczewski, X. Schlagberger, M. Rubinstein, O. Krichevsky, and R. R. Netz, Macromolecules **42**, 860 (2009).
[31]C.-C. Huang, R. G. Winkler, G. Sutmann, and G. Gompper, Macromolecules **43**, 10107 (2010).
[32]T. A. King, A. Knox, W. I. Lee, and J. D. G. McAdam, Polymer **14**, 151 (1973).
[33]M. Adam and M. Delsanti, Macromolecules **10**, 1229 (1977).
[34]T. Nose and B. Chu, Macromolecules **12**, 590 (1979).
[35]C. C. Han and A. Z. Akcasu, Macromolecules **14**, 1080 (1981).
[36]U. Böhme and U. Scheler, Colloids Surf., A **222**, 35 (2003).
[37]K. Grass, U. Böhme, U. Scheler, H. Cottet, and C. Holm, Phys. Rev. Lett. **100**, 096104 (2008).
[38]S. S. Sorlie and R. Pecora, Macromolecules **23**, 487 (1990).
[39]W. Eimer and R. Pecora, J. Chem. Phys. **94**, 2324 (1991).
[40]D. E. Smith, T. T. Perkins, and S. Chu, Macromolecules **29**, 1372 (1996).
[41]R. Götter, K. Kroy, E. Frey, M. Bärmann, and E. Sackmann, Macromolecules **29**, 30 (1996).
[42]A. E. Nkodo, J. M. Garnier, B. Tinland, H. Ren, C. Desruisseaux, L. C. McCormick, G. Drouin, and G. W. Slater, Electrophoresis **22**, 2424 (2001).
[43]E. Stellwagen, Y. Lu, and N. C. Stellwagen, Biochemistry **42**, 11745 (2003).
[44]R. Shusterman, S. Alon, T. Gavrinyov, and O. Krichevsky, Phys. Rev. Lett. **92**, 048303 (2004).
[45]R. G. Winkler, S. Keller, and J. O. Rädler, Phys. Rev. E **73**, 041919 (2006).
[46]E. P. Petrov, T. Ohrt, R. G. Winkler, and P. Schwille, Phys. Rev. Lett. **97**, 258101 (2006).
[47]M. Hinczewski and R. Netz, EPL **88**, 18001 (2009).
[48]A. Bernheim-Groswasser, R. Shusterman, and O. Krichevsky, J. Chem. Phys. **125**, 084903 (2006).
[49]R. G. Winkler, J. Chem. Phys. **127**, 054904 (2007).
[50]C. M. Schroeder, E. S. G. Shaqfeh, and S. Chu, Macromolecules **37**, 9242 (2004).
[51]E. S. G. Shaqfeh, J. Non-Newtonian Fluid Mech. **130**, 1 (2005).
[52]C. M. Schroeder, R. E. Teixeira, E. S. G. Shaqfeh, and S. Chu, Phys. Rev. Lett. **95**, 018301 (2005).
[53]D. Steinhauser, S. Köster, and T. Pfohl, ACS Macro Lett. **1**, 541 (2012).
[54]J. Bonet Avalos, J. M. Rubí, and D. Bedeaux, Macromolecules **24**, 5997 (1991).
[55]V. Lisy, J. Tothova, and A. V. Zatovsky, J. Stat. Mech.: Theory Exp. **2008**, P01024.
[56]T. Franosch, M. Grimm, M. Belushkin, F. M. Mor, G. Foffi, L. Forró, and S. Jeney, Nature (London) **478**, 85 (2011).
[57]U. F. Keyser, Nature (London) **478**, 45 (2011).
[58]B. U. Felderhof, J. Chem. Phys. **123**, 044902 (2005).
[59]M. Belushkin, R. G. Winkler, and G. Foffi, J. Phys. Chem. B. **115**, 14263 (2011).
[60]R. Tatsumi and R. Yamamoto, Phys. Rev. E **85**, 066704 (2012).
[61]S. Henderson, S. Mitchell, and P. Bartlett, Phys. Rev. Lett. **88**, 088302 (2002).
[62]A. Malevanets and R. Kapral, J. Chem. Phys. **110**, 8605 (1999).
[63]R. Kapral, Adv. Chem. Phys. **140**, 89 (2008).
[64]G. Gompper, T. Ihle, D. M. Kroll, and R. G. Winkler, Adv. Polym. Sci. **221**, 1 (2009).
[65]C.-C. Huang, G. Gompper, and R. G. Winkler, Phys. Rev. E **86**, 056711 (2012).
[66]M. Hecht, J. Harting, T. Ihle, and H. J. Herrmann, Phys. Rev. E **72**, 011408 (2005).
[67]J. T. Padding and A. A. Louis, Phys. Rev. E **74**, 031402 (2006).
[68]M. K. Petersen, J. B. Lechman, S. J. Plimpton, G. S. Grest, P. J. in't Veld, and P. R. Schunk, J. Chem. Phys. **132**, 174106 (2010).
[69]A. Lamura, G. Gompper, T. Ihle, and D. M. Kroll, Europhys. Lett. **56**, 319 (2001).
[70]A. Wysocki, C. P. Royall, R. G. Winkler, G. Gompper, H. Tanaka, A. van Blaaderen, and H. Löwen, Soft Matter **5**, 1340 (2009).
[71]I. O. Götze and G. Gompper, EPL **92**, 64003 (2010).
[72]S. P. Singh, R. G. Winkler, and G. Gompper, Phys. Rev. Lett. **107**, 158301 (2011).
[73]D. A. Fedosov, S. P. Singh, A. Chatterji, R. G. Winkler, and G. Gompper, Soft Matter **8**, 4109 (2012).
[74]J. F. Ryder and J. M. Yeomans, J. Chem. Phys. **125**, 194906 (2006).
[75]R. Chelakkot, R. G. Winkler, and G. Gompper, Phys. Rev. Lett. **109**, 178101 (2012).
[76]A. Nikoubashman and C. N. Likos, J. Chem. Phys. **133**, 074901 (2010).
[77]H. Noguchi and G. Gompper, Phys. Rev. Lett. **93**, 258102 (2004).
[78]J. L. McWhirter, H. Noguchi, and G. Gompper, Proc. Natl. Acad. Sci. U.S.A. **106**, 6039 (2009).
[79]T. Ihle and D. M. Kroll, Phys. Rev. E **63**, 020201(R) (2001).
[80]E. Allahyarov and G. Gompper, Phys. Rev. E **66**, 036702 (2002).
[81]L. D. Landau and E. M. Lifshitz, *Fluid Mechanics* (Pergamon Press, London, 1960).
[82]C. M. Pooley and J. M. Yeomans, J. Phys. Chem. B **109**, 6505 (2005).
[83]E. Tüzel, T. Ihle, and D. M. Kroll, Phys. Rev. E **74**, 056702 (2006).
[84]R. G. Winkler and C.-C. Huang, J. Chem. Phys. **130**, 074907 (2009).
[85]R. B. Bird, R. C. Armstrong, and O. Hassager, *Dynamics of Polymer Liquids* (John Wiley & Sons, New York, 1987), Vol. 1.
[86]P. Espanol, Phys. Rev. E **52**, 1734 (1995).
[87]H. Risken, *The Fokker-Planck Equation* (Springer, Berlin, 1989).
[88]I. S. Gradshteyn and I. M. Ryzhik, *Table of Integrals, Series, and Products* (Academic Press Inc., San Diego, 1980).
[89]R. G. Winkler, Soft Matter **6**, 6183 (2010).
[90]M. P. Allen and D. J. Tildesley, *Computer Simulation of Liquids* (Clarendon Press, Oxford, 1987).
[91]C.-C. Huang, A. Chatterji, G. Sutmann, G. Gompper, and R. G. Winkler, J. Comput. Phys. **229**, 168 (2010).
[92]A. Malevanets and J. M. Yeomans, Europhys. Lett. **52**, 231 (2000).
[93]E. Westphal, S. P. Singh, C.-C. Huang, G. Gompper, and R. G. Winkler, "GPU accelerated particle-based mesoscale hydrodynamic simulations—multiparticle collision dynamics and its application to star-polymer diffusion" (unpublished).
[94]B. Dünweg and K. Kremer, J. Chem. Phys. **99**, 6983 (1993).
[95]P. Ahlrichs and B. Dünweg, J. Chem. Phys. **111**, 8225 (1999).
[96]C. Pierleoni and J.-P. Ryckaert, J. Chem. Phys. **96**, 8539 (1992).
[97]I.-C. Yeh and G. Hummer, J. Chem. Phys. B **108**, 15873 (2004).
[98]A. J. C. Ladd, R. Kekre, and J. E. Butler, Phys. Rev. E **80**, 036704 (2009).
[99]A. A. Zick and G. M. Homsy, J. Fluid Mech. **115**, 13 (1982).